Preprint PFC/JA-84-41

MICROWAVE STUDIES OF A TUNABLE FREE ELECTRON LASER IN COMBINED AXIAL AND WIGGLER MAGNETIC FIELDS

J. Fajans, G. Bekefi, Y.Z. Yin, and B. Lax

Plasma Fusion Center and
Research Laboratory of Electronics
Massachusetts Institute of Technology
Cambridge, MA. 02139

December 1984

Microwave Studies of a Tunable Free Electron Laser in Combined Axial and Wiggler Magnetic Fields

J. Fajans, G. Bekefi, Y.Z. Yin[†], and B. Lax

Department of Physics and Research Laboratory of Electronics

Massachusetts Institute of Technology

Cambridge, MA 02139

Abstract

We report narrow band ($\Delta\omega/\omega \leq 0.02$) microwave emission from a tunable ($7 \leq \omega/2\pi \leq 21$GHz) Raman, free electron laser operating in a single TE_{11} waveguide mode. Approximately 100kW of RF power has been observed at an electronic efficiency of 12%, and $\sim$ 1MW of RF power has been generated at a reduced efficiency of 8%. Frequency, gain and RF power measurements have been carried out for various values of the guide magnetic field, below, above and near to the resonance between the cyclotron frequency of the guide magnetic field and the frequency associated with the periodic wiggler magnetic field. The results are in very good agreement with the predictions of three-dimensional free electron laser theory.

[†]Permanent address: Institute of Electronics, Academia Sinica, Beijing, People's Republic of China.

I—Introduction

The Raman (collective) free electron laser (FEL) produces coherent radiation by subjecting a cold, intense electron beam to a periodic "wiggler" magnetic field. The wiggler magnet causes the electron beam to oscillate transversely, and this periodic oscillation couples via the ponderomotive force[1-3] to a longitudinal beam space charge (plasma) oscillation. The net induced oscillating current drives the coherent output radiation, with the energy for the radiation coming at the expense of the beam kinetic energy. The outstanding properties of the FEL include its inherent tunability, high radiation levels and moderately good efficiencies.

Theory predicts radiation at two frequencies approximately given by $\omega = \beta_{\|} c k_w \gamma_{\|}^2 (1 \pm \beta_{\|})$, where $\gamma_{\|} = (1 - \beta_{\|}^2)^{-1/2}$ is the relativistic axial energy factor, $\beta_{\|} = v_{\|}/c$ is the normalized axial velocity of the electron beam, and $k_w = 2\pi/l$, where l is the wiggler period. Consequently the FEL can be tuned by changing the accelerator voltage. Promise of wide tunability merely by changing the accelerator voltage gives the FEL one of its most distinguishing characteristics.

A focusing guide magnetic field $B_{\|}$ is utilized to contain the unneutralized beam. This additional field results in an interesting "resonant" regime much explored by theorists[4-7] which occurs in a parameter regime $\Omega_{\|}/\gamma \approx k_w \beta_{\|} c$, where $\Omega_{\|} = eB_{\|}/m_0$ is the non-relativistic cyclotron frequency in the axial guide magnetic field and γ is the total relativistic energy factor $\gamma = 1 + eV/m_0c^2 =$

$(1-\beta_{\|}^2-\beta_{\perp}^2)^{-1/2}$ with V as the accelerator voltage. Use of an electron gun with a thermionic cathode permits long pulse operation of the FEL and yields a low temperature beam ($\Delta\gamma_{\|}/\gamma \approx 3\times 10^{-3}$).

In this paper we describe a detailed experimental study of a free electron laser operating at mildly relativistic energies $V \approx 175$kV, $\gamma \approx 1.35$, sometimes referred to as the Ubitron regime.[8] We demonstrate[9] continuous, narrow-band, single mode tuning from 7 to 21GHz, and we believe that this is the first detailed study of the frequency versus voltage tuning of both the high and the low frequency branches of the FEL instability mentioned above under high current density, collective (Raman) operation.

Our FEL is used both as an oscillator and as an amplifier. In the oscillator mode, the FEL generates over 100kW of power at an electronic efficiency of twelve percent. The amplifier mode gain is measured as a function of wiggler strength and a maximum gain of 20dB is achieved. Our measurements are conducted for a variety of guide magnetic fields, well below, well above, and also in the immediate vicinity of the above mentioned resonance $\Omega_{\|}/\gamma = k_w\beta_{\|}c$. Comparison of our results with theoretical predictions provides the first detailed confirmation of the Raman FEL dispersion and orbit theory. We find that in several instances comparison has to be made with recently developed three dimensional theories[10-11] which take proper account of the finite transverse dimensions of the waveguide and the electron beam, and the radial variation of the wiggler field

amplitude.

In section II of this paper we describe the experimental arrangement. In section III we summarize the theoretical results needed to interpret the measurements described in section IV. Section V summarizes our findings and compares them with the work of others.

II—Experimental Arrangement

A schematic of the FEL is shown in Figure 1. The accelerating potential for the laser is supplied by a Marx generator (Physics International Pulserad 615MR, which has a maximum capability of 500kV and 4kA.). Unlike most of the accelerators used in previous mildly relativistic FEL experiments,[12–14] the 615MR does not use a pulse-forming network. Consequently the output voltage pulse is essentially that of a discharging capacitor bank ($C = 0.083\mu$F) with a shunt adjusted RC time constant of 10–100μs. The output voltage is monitored by a carefully calibrated resistive divider network. (The calibration error is estimated to be less that two percent.) Because the FEL's properties depend strongly on the electron beam voltage, the essentially flat, noise-free voltage pulse produced by the 615MR proves to be very important, and represents a substantial improvement over the capabilities of earlier experiments.

The electron beam is generated by a thermionically emitting, electrostatically focused, Pierce type electron gun (250kV, 250A) removed from a SLAC klystron (model 343). An assembly of six focusing coils is designed so that their magnetic

field lines lie along the zero-magnetic-field electron trajectories.[15] This field configuration gives the least scalloping of the electron beam (low transverse temperature) and allows the magnetic field amplitude to be varied over a wide range without greatly affecting the electron beam temperature. Only the inner portion of the beam is used; an aperture limits the beam radius to $r_b = 0.254$cm. The aperture scrapes off the outer electrons which exhibit significant scalloping, and it limits the product $k_w r_b$ to less than 0.5, which is desirable[16] in order to ensure good helical orbits. Consequently, the net current entering the magnetic wiggler is in the range of 1—8A.

A typical gun simulation obtained with the Stanford Electron Optics[17] computer code is shown in Figure 2. The simulations indicate that the perpendicular energy of the transmitted electrons at radii $r \leq r_b$ is always less than 0.2% of their total energy throughout the range of experimentally possible axial field values $0.5\text{kG} \leq B_{||} \leq 7\text{kG}$. The code predicts that the perpendicular energy of the electrons in the beam is in the form of coherent scalloping in the beam radius. Since the scalloping frequency is approximately given by the cyclotron frequency $\Omega_{||}/\gamma$, the scalloping wavelength is $2\pi\beta_{||}c\gamma/\Omega_{||}$. Because of the slow voltage decay inherent to our accelerator, the axial velocity $\beta_{||}$ and the scalloping wavelength decrease during a shot, and the radius of the beam oscillates at any fixed downstream location. This oscillation modulates the current transmitted through the limiting aperture. By measuring the amplitude of the current modulation, the

perpendicular energy $\Delta E_\perp \simeq \frac{1}{2} m_0 \Delta v_\perp^2 \gamma_\parallel^3$ of the beam due to scalloping can be inferred in a manner similar to that employed previously.[12,18] The perpendicular energy of our beam thus determined is studied for various axial magnetic fields $B_\parallel$ (Figure 3), and is seen to be in good agreement with the perpendicular energy predicted by the computer simulations. The maximum amount of perpendicular energy occurs at $\Omega_\parallel/\omega_p\gamma^{1/2} \simeq 10$, where $\Omega_\parallel$ and the nonrelativistic plasma frequency $\omega_p = (Ne^2/m_0\epsilon_0)^{1/2}$ are measured in the drift tube region. However, near the cathode, where the scalloping is generated, $\Omega_\parallel$ and ω_p are lower, and the corresponding ratio $\Omega_\parallel/\omega_p\gamma^{1/2} \simeq 2.5$. This is close to the classical Brillouin condition[19] at $\Omega_\parallel/\omega_p\gamma^{1/2} \simeq 1.4$ that separates electrostatically dominated beam propagation from magnetically dominated beam propagation.

We emphasize that this diagnostic measures only one component of the beam temperature, namely coherent scalloping. Other sources of temperature include whole beam rotations[19], noncoherent scalloping, and gun dependent emittance phenomena. The latter can be estimated by means of the semi-empirical Lawson-Penner[20] condition which, for our gun, yields an normalized emittance of ~ 0.02rad-cm. This emittance corresponds[20] to an axial energy spread $\Delta\gamma_\parallel/\gamma$ of approximately 0.3 percent. The wiggler itself adds temperature to the beam because of the radial inhomogeneities of the wiggler field; however this effect gives an energy spread substantially less than 0.1 percent. It is difficult to determine the effect of the wiggler entrance on the beam temperature, but theoretical studies and numeric work indicate that the temperature increase is

small far from the axial field resonance.[4,21]

The gun focusing coils guide the electron beam into a 2.54cm ID stainless steel evacuated drift tube. The beam is contained by a uniform axial magnetic field $B_{\|}$ that has a power supply limited maximum of 7kG, and a Brillouin flow minimum of approximately 800G (below which beam defocusing and deterioration occurs). The current is measured before and after the wiggler by Rogowski coils that are calibrated to an accuracy of five percent. When the electron gun operates in the Child-Langmuir space charge limited regime, the gun perveance is approximately 0.4μpervs. At 250kV, the maximum current density is 50Acm^{-2}. In certain studies it is sometimes desirable to change the current density. This is accomplished by lowering the cathode heater current and thereby go from the space charge limited regime of gun operation to the temperature limited regime.

Since operation always occurs at a current level much below the drift tube limiting current,[22] the space charge depression from the drift tube wall to the beam center is small and does not exceed 1800V. Consequently the effect of the beam space charge depression on the electron energy can be ignored, and the beam γ is given to good accuracy by $\gamma = 1 + eV/m_0c^2$, where V is the accelerator voltage.

In contrast to most previous Raman FEL experiments[12–14] which use field emission or plasma flash-over cathodes, we use an electron gun that employs an oxide coated, thermionically emitting cathode. This allows long pulse operation

because there is no diode closure due to plasma motion, which normally limits field emission diodes to pulse lengths of less than $\sim$ 100ns.

Thermionic cathodes require a clean environment, and cold cathode base pressures of $\sim 5 \times 10^{-8}$Torr must be maintained. To this purpose the cathode anode gap insulator is comprised of a brazed metal to ceramic cylinder. Metal gaskets are used wherever possible, and the system is baked out before and during cathode activation. The electron gun is continuously pumped by a Vac Ion pump, and is separated from the rest of the system by a gate valve which is only open during FEL operation. With the cathode fully emitting, the system pressure is less than 3×10^{-7}Torr.

The 50 period circularly polarized magnetic wiggler has a period $l =$ 3.3cm $(k_w = 2\pi/l = 1.90)$, a maximum amplitude $B_w = 1.5$kG, and is generated by bifilar conductors[23–25] wound directly on the outside of the stainless steel drift tube. Since the beam aperture limits the size of the beam to $k_w r_b = 0.5$, the wiggler field is close to that of an ideal wiggler. That is, the effects of the radial variation of the wiggler field and the presence of the off-axis components are usually small (but see below). At the wiggler entrance, a slowly increasing wiggler field amplitude is produced by resistively loading the first six periods of the wiggler magnet.[26] The resistive loads consist of nichrome loops placed every half period that connect the two wires in the bifilar windings. The entrance profile illustrated in Figure 4 is generated by using 13 loops with normalized resistances

of 4.0, 2.5, 2.5, 1.6, 1.6, 1.0, 1.0, 1.0, 1.6, 1.6, 2.5, 2.5, 4.0.

The 2 meter long, 2.54cm ID drift tube acts as a cylindrical waveguide whose fundamental TE_{11} mode has a cutoff frequency of $\omega_{c0}/2\pi = 6.92$GHz. A vacuum window transmits the circularly polarized FEL radiation propagating in the drift tube into a broadband TE_{11} circular guide to a TE_{10} rectangular guide transformer, which couples the FEL emission out of the system in the form of a linearly polarized wave traveling in the rectangular guide. The low conductivity of the stainless steel drift tube attenuates the microwave signal by approximately 0.3 dB per meter.

III—Theoretical Considerations

The emission from a Raman free electron laser results from the interaction between the slow space charge wave on the electron beam

$$\omega = \beta_{\|} c(k + k_w) - p_1 \omega_p \Phi^{1/2} / \gamma^{1/2} \gamma_{\|} \tag{1}$$

and the electromagnetic waveguide mode

$$\omega^2 = c^2 k^2 + \omega_c^2. \tag{2}$$

Here ω and k are the output radiation frequency and wave number, respectively; $\omega_p = (Ne^2/m_0\epsilon_0)^{1/2}$ is the nonrelativistic plasma frequency; $\omega_c = \left[\omega_{c0}^2 + p_2^2 \omega_p^2/\gamma\right]^{1/2}$ is the effective waveguide cutoff frequency adjusted for the presence of the electron beam; ω_{c0} is the empty waveguide cutoff frequency; p_1 and p_2 are frequency dependent numerical factors,[27–29] less than unity that are related to the finite transverse geometry of the waveguide; and Φ is a correction to the

space charge dispersion equation due to the combined presence of the axial and wiggler magnetic fields, defined as[6]

$$\Phi = 1 - \{\Omega_{\|}\gamma_{\|}^2\beta_w^2/[(1+\beta_w^2)\Omega_{\|} - k_w\beta_{\|}c]\}, \tag{3}$$

where $\beta_w = \beta_\perp/\beta_{\|}$, and $\beta_\perp = v_\perp/c$ is the normalized transverse velocity acquired by the electrons from the wiggler magnetic field. Depending on the parameters of the experiment, Φ can be positive, negative, or zero.

Maximum gain of the FEL instability occurs near the frequency ω corresponding to the crossing points of the space charge and electromagnetic modes. Solving Eqs. (1) and (2) leads to the radiation frequency

$$\omega = \beta_{\|}ck_{w\text{eff}}\gamma_{\|}^2\left\{1 \pm \beta_{\|}\left[1 - \left(\omega_c/k_{w\text{eff}}\gamma_{\|}\beta_{\|}c\right)^2\right]^{1/2}\right\} \tag{4}$$

where the effective wiggler wave number $k_{w\text{eff}} = k_w - p_1\omega_p\Phi^{1/2}/\gamma^{1/2}\gamma_{\|}\beta_{\|}c$, and where the $\pm$ selects the high and low frequency branches of the FEL instability, respectively. For most, but not all of our operating regimes $\omega_p/\gamma^{1/2}\gamma_{\|}\beta_{\|}c \ll k_w$, $\Phi \approx 1$, and the reduction p_1 in the plasma frequency due to the "drag" of the waveguide wall is approximately 0.5. Thus the w_p dependent terms are generally small and $k_{w\text{eff}} \simeq k_w$. Likewise $\omega_c \simeq \omega_{c0}$, because p_2, which is approximately equal to the electromagnetically weighted ratio of the area of the electron beam to the cross-sectional area of the waveguide, is much less than one.

To find the FEL output frequency as a function of the magnetic fields $B_{\|}$, B_w, and the beam energy γ, it is necessary to determine the axial velocity $\beta_{\|}$

of the electrons in the beam. Calculations and computer simulations show that the electrons in a high quality electron beam launched into a wiggler magnet travel at approximately constant axial velocity if the wiggler has a slow (adiabatic) entrance and if the wiggler and axial fields are not too near resonance.[4,21] In a one-dimensional theory employing an idealized wiggler

$$\vec{B}_w = B_w(\hat{x}\cos k_w z + \hat{y}\sin k_w z), \tag{5}$$

and a constant axial field $\vec{B}_{\|} = \hat{z}B_{\|}$, the axial velocity $\beta_{\|}$ for a constant velocity orbit can be found by simultaneously solving the energy conservation relation[4]

$$1/\gamma^2 = 1 - \beta_{\|}^2 - \beta_{\perp}^2, \tag{6}$$

and the equation for the electron's perpendicular velocity

$$\beta_{\perp} = |\Omega_w \beta_{\|}\left[\gamma k_w \beta_{\|} c - \Omega_{\|}\right]^{-1}|; \qquad (\gamma k_w \beta_{\|} c \neq \Omega_{\|}). \tag{7}$$

Here $\Omega_w = eB_w/m_0$ is the nonrelativistic cyclotron frequency in the wiggler magnetic field. Resonance occurs when the denominator of Eq. (7) becomes small. Close to resonance the perpendicular velocity and the radial excursions of the electrons in the beam become large, and the idealized theory based on Eqs. (6) and (7) is no longer valid.

Equations (6) and (7) together form a single fourth order polynomial for $\beta_{\|}$. The solutions of this polynomial can be divided into two regimes.[4,5,30] The so called group I regime is found when $B_{\|}$ is small and γ is large such that $\Omega_{\|}/\gamma < k_w \beta_{\|} c$ (below resonance), and the group II regime is found when $B_{\|}$ is large and γ is small such that $\Omega_{\|}/\gamma > k_w \beta_{\|} c$ (above resonance).

In our experiments the axial and wiggler magnetic fields are usually held fixed while and the energy γ is varied. Figure 5 shows the variation of $\beta_{||}$, (and consequently the output frequency ω), with energy γ. When an electron is launched into a wiggler in an adiabatic manner, it will enter the orbit with the highest possible value of $\beta_{||}$. Thus, the orbits indicated by the dashed lines in Figure 5 are inaccessible, and, for a given set of magnetic field values, there exists a region of axial velocities (and hence output frequencies) that is not accessible for any energy. As γ is lowered, the axial velocity $\beta_{||}$ for an electron in a Group I trajectory decreases monotonically until the orbit type disappears abruptly. Group II orbits, however, exhibit a maximum in $\beta_{||}$ at the value $\gamma^2_{\text{crit}} = p + (\Omega_{||}/k_w cp)$ where $p = 1 + (\Omega_w/k_w c)^{2/3}$. Therefore there must be a region in which $\beta_{||}$, and thus also the FEL radiation frequency *decrease* when γ increases. We note that several earlier experiments have operated in this "anomalous" region.[14,31,32] Since in this region $d\beta_{||}/d\gamma \approx 0$, frequency tuning of the FEL by varying γ is no longer possible, and tuning by variation of B_w had to be employed.[31] However, this lack of tunability is offset by high predicted efficiencies,[34] and any large energy spread in the beam may also affect the radiation bandwidth less severely. We note that this region corresponds to the case where Φ of Eq. (3) is less than zero.

Since the FEL output frequency is a very sensitive function of $\beta_{||}$, the one-dimensional, ideal wiggler theory based in Eqs. (5) and (7) is often inadequate, because, when $r \neq 0$, the radial field component of a "realistic" wiggler increases in strength and B_w acquires an axial component. Thus, for off axis particles, B_w

becomes a function of r and Eq. (7) must be corrected for the more realistic field, which in a cylindrical coordinate system $(\hat{\mathbf{e}}_r, \hat{\mathbf{e}}_\theta, \hat{\mathbf{e}}_z)$, is given by[16]

$$\mathbf{B}_w = 2B_w\Big(\hat{\mathbf{e}}_r I_1'(k_w r)\cos(\theta - k_w z) + \hat{\mathbf{e}}_\theta \frac{I_1(k_w r)}{k_w r}\sin(\theta - k_w z) + I_1(k_w r)\hat{\mathbf{e}}_z \sin(\theta - k_w z)\Big) \quad (8)$$

where I_1 is the modified Bessel function. However, there nevertheless exists a class of axis-encircling trajectories that are very similar to the orbits in the idealized wiggler, and Eq. (7) now becomes,[30]

$$\beta_\perp = |\beta_w|, \quad \beta_w = \frac{2\Omega_w \beta_\parallel I_1(\lambda)/\lambda}{\gamma k_w \beta_\parallel c - \Omega_\parallel - 2\Omega_w I_1(\lambda)}. \quad (9)$$

Here $\lambda = \beta_w/\beta_\parallel = \pm k_w r$ is the normalized size of the orbit, such that $\lambda = -k_w r$ when $\Omega_\parallel \gamma < k_w \beta_\parallel c$ and $\lambda = +k_w r$ when $\Omega_\parallel \gamma > k_w \beta_\parallel c$.

To determine the strength of the FEL interaction, it is necessary to determine the FEL operating regime; namely whether the experiment is in the single particle, low gain, Compton regime, or in the desirable high gain collective Raman regime. To be in the latter, it is required that, in the frame of the moving electrons, the wavelength of the space charge wave be greater that the Debye length.[35] In the laboratory frame this translates into the inequality[29]

$$\Delta\gamma_\parallel/\gamma < \frac{p_1 \omega_p}{\omega \gamma^{1/2}} \gamma_\parallel \beta_\parallel^2. \quad (10)$$

For our parameters, the right hand side of the above equation equals ~ 0.02. The computer simulations and experiments show that $\Delta\gamma_\parallel/\gamma \leq 0.003$, and the inequality is well satisfied. If the wiggler field is very strong the FEL enters the so

called "strong pump" regime. In our experiment the wiggler strength and thus the electron undulations are always so small that the "strong pump" inequality,[2]

$$\frac{p_1\omega_p}{\omega\gamma^{3/2}} \ll p_2\beta_\perp^2$$

is never satisfied.

To calculate the FEL gain, one must solve the complete, coupled dispersion relation. In the Raman regime, the FEL dispersion relation is of the form

$$D_{SP}^{slow} D_{SP}^{fast} D_{EM} = \tilde{\Gamma}_0^2. \tag{11}$$

Here D_{SP}^{slow} and D_{SP}^{fast} are the dispersion relations of the the uncoupled slow and fast space charge waves upshifted in frequency by the wiggler wavenumber k_w; and D_{EM} is the dispersion relation of the uncoupled electromagnetic wave. $\tilde{\Gamma}_0$ is the coupling coefficient which determines the gain. Maximum gain in obtained when D_{SP}^{slow} and D_{EM} are approximately zero, and, in one dimensional theories the electric field gain is approximately,[36]

$$\Gamma = \frac{1}{2}\frac{\beta_\perp}{\beta_\parallel}\gamma_\parallel\left[p_2\frac{p_1\omega_p k_w}{\gamma_\parallel\gamma^{1/2}c}\Phi^{1/2}\right]^{1/2}. \tag{12}$$

The linear increase with $\beta_\perp$ and the increase with beam current as $\omega_p^{1/2}$ are characteristic of the Raman regime. Since $\beta_\perp$ is approximately proportional to B_w (Eq. (7)), the gain also increases nearly linearly with B_w, in agreement with observations discussed in section IV-3.

The effect of damping and beam temperature can be found, to first order, by inserting damping rates into the dispersion relations D_{SP} and D_{EM}. The EM

wave damping rate is due to the attenuation of the waveguide wall. The space charge wave damping rate is a combination of Landau damping[37] and waveguide damping. For our beam, the effects of these damping terms are found to be small.

IV—Experimental Results and Comparison with Theory

In this section we present our experimental results for the oscillator mode of operation in which the signal grows out of the background noise, and for the amplifier mode of operation in which a monochromatic signal of known amplitude and frequency is injected into the wiggler region.

(1) Threshold and Power Measurements in the Oscillator Mode

When the wiggler field is increased above a threshold value, the FEL radiates spontaneously. A typical shot is shown in Figure 6. When the Marx bank fires, the gun voltage rises rapidly to about 200kV and then "RC" decays towards zero. The beam current roughly parallels the voltage behavior, attaining a maximum current of 7A. When the voltage decays to about 160kV, a 2μs burst of microwaves is observed. The microwave signal ends when the voltage is so low that the phase velocity of the upshifted space charge wave can no longer travel in synchronism with the TE_{11} electromagnetic waveguide mode.

The exact value of the oscillation threshold for the wiggler field depends on the beam current, the voltage decay rate, the axial magnetic field strength, and the percentage of microwave power that is reflected back into the system. Far from resonance it is generally in the range of 100-200G. When the wiggler

is raised above the threshold wiggler field the output power rises extremely sharply and quickly saturates. A typical case is shown in Figure 7a, in which the total microwave power above a frequency of 7GHz is plotted as a function of the wiggler field strength B_w. Below threshold, there is no measurable power. Radiation is first observed at $B_w = 125$G, and the output power climbs over eight orders of magnitude before saturating at $B_w = 180$G.

Although the microwave output power shown in Fig. 7a has not been spectrally resolved, most of the observed emission is believed to originate when the conditions for maximum gain prevail, namely at the point of grazing incidence intersection between the space charge and electromagnetic modes. For this to occur Eq. (4) shows that

$$\beta_{\|}\gamma_{\|} = \frac{\omega_c}{k_{w\text{eff}}c} \tag{13}$$

and

$$\omega = \gamma_{\|}\omega_c. \tag{14}$$

It therefore follows from Eqs. (7) and (13) that as the wiggler field B_w is increased, the radiation peak occurs at ever higher accelerator voltages V. This is illustrated in Fig. 7b. We see good agreement between the experiment and the theoretical prediction obtained by solving Eqs. (7) and (13).

Microwave power is measured by extracting a small fraction of the FEL output radiation with a directional coupler, with the remainder of the radiation terminated in a standard microwave load. The extracted signal is further reduced

by attenuators and is measured by a calibrated crystal diode detector. To prevent arcing at high power levels, the microwave components are pressurized with sulphur hexafluoride.

We observe[9] 100kW of RF power when a 160kV, 5.1A electron beam is allowed to enter the wiggler interaction region. This corresponds to a beam current density of $20A/cm^2$ and an electronic efficiency of 12% of converting beam power to radiation. The computed saturated efficiency governed by electron trapping in the ponderomotive potential wells is approximately 15%.

Considerably more power can be obtained at the expense of FEL efficiency. The fields of the focusing coils (see Fig. 1) can be changed to overfocus the electron beam, thereby increasing the current passing through the limiting aperture. Unfortunately, this also increases the beam scalloping and temperature. In this mode of operation, we observe as much as 1MW of RF power with a beam current of 50A. We note that the cold beam theoretical efficiency has substantially increased from the previous value of 15%; however, the measured efficiency is down to 8%. This drop in efficiency is consistent with theoretical work[38] which indicates that the FEL efficiency is depressed by high temperature electron beams.

(2) Frequency Characteristics in the Oscillator Mode

An X-band (8-12Ghz), dispersive line is used to determine the frequency of the output radiation.[39] A broadband p-i-n diode microwave switch (Alpha

Industries MT8675H) is used to limit the long duration microwave signal to 15ns. The frequency is determined by displaying the undispersed signal and the dispersed output signal on a fast oscilloscope (Figure 8), and computing the frequency from the time difference between the two signals. Normally, only the high frequency upshifted microwave signal is observed; however occasionally signals from both roots of Eq. (4) are observed simultaneously (Figure 8b). The frequency bandwidth can be estimated by measuring the width of the dispersed signal. The width thus determined is about two percent.

The dependence of the output frequency on the beam energy γ is found to agree well with the frequencies predicted from Eq. (4) , as is illustrated in Fig. 9. Measurements are shown for two different values of the wiggler field amplitude. Note that both the upshifted and the downshifted branches are observed, and that the two branches merge at a frequency somewhat above the cutoff frequency ω_c of the TE_{11} mode. Frequency tuning can be accomplished directly by varying the beam energy or indirectly by varying the wiggler strength. However, frequency tuning by varying B_w is not a desirable technique because of the strong dependence of the FEL gain on the value of B_w (see Eq. (12)).

(3) Gain and Frequency Characteristics in the Amplifier Mode

When the FEL is operated with the wiggler field below its spontaneous threshold value, the FEL can be used as an amplifier. A low level (0.1—1.0W) monochromatic CW signal of the known frequency $\omega/2\pi$ is sent into the drift

tube from the direction of the microwave output window. The signal propagates through the wiggler anti-parallel to the electron beam, and is then reflected back through the system in the forward direction by the beam aperture (a wire mesh microwave mirror is inserted occasionally to improve the reflectivity). Figure 10 illustrates a typical shot. Since the accelerator has an RC droop, the beam energy sweeps through a range of values as seen in Figure 10a. Amplification occurs (Figure 10b) at the time during the voltage pulse when the voltage reaches the appropriate value as predicted by Eq. (4) . In addition to wave growth, one can also obtain wave damping in which energy from the wave is converted into kinetic energy of the electrons. This wave damping is also illustrated in Fig. 10b, and is attributed to an interaction with the fast space charge wave, as is discussed in subsection 4.

To assure ourselves that proper amplification does in fact occur, we measure the RF output power as a function of the RF input power, as is illustrated in Fig. 11. The FEL gain (ratio of power in to power out) is constant over a 30dB range of input signals.

In order to compare the experimentally observed gain with the theoretically predicted gain, it is desirable to determine the gain for a single forward traversal of the incident electromagnetic wave. (We note that more than one pass may have occurred in Figs. 10 and 11.) To measure the single pass gain, the system is driven with a train of short (< 15ns), well separated pulses. As can be seen in Figure

12, the interval during which the voltage is appropriate for the input frequency lasts about 300ns. The small increase in the microwave baseline indicates that the imperfect nature of the output components cause reflections and cause a low residual level of microwaves to circulate in the system. However, since the individual microwave pulse lengths are less than the system bounce time, the single pass gain can be immediately determined by measuring the height of the microwave pulse over the baseline. This measurement technique also precludes the possibility that the signal being measured is the that of a triggered oscillator.

The measurements of gain as a function of wiggler strength B_w is shown in Fig. 13 under conditions of constant input frequency, beam current and axial guide field $B_{\|}$. Such a study provides a sensitive test of FEL theory. To factor out the effect of the waveguide attenuation, the gain is calculated as the ratio of the amplified P_{out} to the P_{out} when the beam is not present. Because the system oscillates spontaneously at high wiggler fields, the gain could not be measured above 20dB. The experimental results are seen to be in good agreement with three dimensional theory.[10] At high values of the wiggler field, the gain increases linearly as is characteristic of the Raman regime, and at low wiggler values, the gain exhibits launching losses described below. We note that one dimensional theories (Eq. (12)) give a value of the gain that is too low, for example, by about 14dB at $B_w = 230\text{G}$. Therefore our results tend to confirm three dimensional theoretical studies.

As noted above, the experimental gain depends on the wave launching conditions. We launch a linearly polarized wave; however, helical wiggler FELs are thought to amplify a circularly polarized wave. Under the assumption of no Faraday rotation, this reduces the observed gain of the FEL from $P_{out} = P_{in}\exp(2\Gamma z)$ to $P_{out} = P_{in}[\exp(\Gamma z)/2 + 1/2]^2$. Moreover, theory predicts that two waves of equal magnitude are launched; one corresponding to the growing solution of the dispersion equation, and one corresponding to the complex conjugate, decaying solution.[29] Thus the power gain is further reduced, with the result that $P_{out} = P_{in}[\exp(\Gamma z)/4 + \exp(-\Gamma z)/4 + 1/2]^2$. When Γ is large, this last formula is identical to the above single wave formula $P_{out} = P_{in}\exp(2\Gamma z)$ with the addition of a 12dB launching loss; however, when Γ is small, the linear terms in the gain expression cancel, and the gain increases *quadratically* with Γ. Consequently, until $\Gamma z \gtrsim 0.5$ there is effectively no gain. The exact value of the gain depends on the length of the wiggler and the wiggler strength in the introduction region; in the gain calculations we use an effective, constant amplitude wiggler length of 47.25 periods. The small differences between theory and experiment seen in Fig. 13 are being studied.

By varying the injected input frequency and measuring the voltage at which amplification occurs, the frequency-voltage characteristics of the FEL can be determined. Amplification is observed from 7 to 21GHz, as is illustrated in Figure 14. Agreement with theory is excellent. The continuous tuning of the FEL over a factor of three in frequency confirms the versatility of this type of device. We

note that gain is readily observed for both the low and high frequency branches of the FEL instability, and for low and high values of the guide magnetic field $B_{\|}$.

In the presence of a guide magnetic field the cyclotron maser instability may well be excited and compete with the FEL instability.[40] To guard against this possibility, one must try to suppress the cyclotron maser instability by operating the FEL without a guide magnetic field or by using a guide field that is so low that the fundamental cyclotron frequency is cut-off by the microwave waveguide. If such schemes are not feasible, one must assure that the FEL instability frequency is far removed from the cyclotron instability frequency. In our "below resonance curve", for example, (Figure 14), the fundamental cyclotron mode is below the waveguide cutoff. The upshifted second harmonic would extend in a nearly straight line from $f = 15\text{GHz}$ at $\gamma = 1.26$ to $f = 19\text{GHz}$ at $\gamma = 1.46$. Since in our experiments, the cyclotron instability is, in general, far from the FEL instability, it is unlikely to interfere with FEL operation.

(4) Plasma Frequency Effects and Damping of the Fast Space Charge Wave

The beam density affects the FEL emission frequency by causing a change in the effective wiggler period, $k_{w\text{eff}} = k_w - p_1\omega_p\Phi^{1/2}/\gamma^{1/2}\gamma_{\|}\beta_{\|}c$ of Eq. (4) . Consequently high beam densities depress the output frequency. The decrease in $k_{w\text{eff}}$ due to the correction term $p_1\omega_p\Phi^{1/2}/\gamma^{1/2}\gamma_{\|}\beta_{\|}c$ is typically less than six percent in all of our experiments. This decrease is shown Figure 15 in which we

determine the beam energy γ required for the FEL to amplify the fixed frequency $\omega/2\pi = 12.02$GHz, as a function of the plasma frequency. The plasma frequency itself is varied by controlling the beam current by adjusting the thermionic cathode temperature. We note that the good agreement between the data and the theoretical predictions confirms that the FEL is indeed operating in the Raman (collective) region, because the plasma wave correction to the output frequency of a Compton regime FEL is determined (to first order) by the beam temperature rather than the beam density.[3]

Gain is observed in the free electron laser instability when the EM wave interacts with the slow space charge wave. Damping will result if the interaction is with the fast space charge wave; here the dispersion relation Eq. (11) is solved with D_{EM} and $D_{\mathrm{SP}}^{fast} \approx 0$. The downward directed microwave pulse in Fig. 10b shows that wave damping occurs at a slightly lower electron beam energy than does wave growth. This agrees with expectations since wave growth or damping depend on the electron velocity relative to the phase velocity of the ponderomotive wave. We speculate that the energy removed from the EM wave is added to the beam energy, and that this effect corresponds to the predicted inverse free electron laser acceleration effect.

Compiling data like that shown in Fig. 10, we show in Fig. 15a the energy required to damp a fixed frequency wave as a function of the plasma frequency. As expected the difference in energy between growth and damping increases as

the plasma frequency is increased. This comes from the fact that the slow and fast space charge waves (cf Eq. (1)) differ in sign only, namely,

$$\omega = \beta_{\|} c(k + k_w) \mp p_1 \omega_p \Phi^{1/2} / \gamma^{1/2} \gamma_{\|}. \tag{15}$$

The agreement with theory for wave damping is seen to be as good as for wave growth.

(5) Measurements near Resonance, $\Omega_{\|}/\gamma \simeq k_w \beta_{\|} c$

Near resonance, it is much harder to launch an electron into a constant $\beta_{\|}$ orbit because the conditions on the initial beam temperature, the beam radius, and the wiggler entrance adiabaticity are more stringent. In addition, there exist certain values of the magnetic fields in which an electron entering a wiggler is forced to undergo a transition from a Group I ($\Omega_{\|}/\gamma < k_w \beta_{\|} c$) to a Group II ($\Omega_{\|}/\gamma > k_w \beta_{\|} c$) orbit. This can occur for axial magnetic fields just above resonance, because the type of orbit depends on the wiggler strength. Consequently, at the wiggler entrance, where the wiggler magnetic field B_w is small, the electrons will be in a Group I orbits, but in the middle of the wiggler, where B_w is large, the electrons will be in an approximate Group II orbit.[4] At some critical value of the wiggler field the electron will be forced to undergo a transition between the two groups. At this transition point the axial velocity $\beta_{\|}$ for the two orbits will be mismatched by an amount $\Delta\beta_{\|}$I-II, and this mismatch in the electron velocity will induce large oscillations in $\beta_{\|}$. The lower quality, large radius orbits will cause a fraction of the electrons to hit the drift tube wall, causing the current in the wiggler region to decrease.

This decrease in the current near resonance is verified experimentally by measuring the transmitted current while varying the total energy γ at a fixed axial magnetic field $B_{||} = 2310G$ and wiggler amplitude at $B_w = 160G$ (Figure 16). The transmitted current at each energy is normalized to the current transmitted with the wiggler turned off. As indicated by I and II in the figure, the electrons are in Group I (II) orbits above (below) $\gamma \simeq 1.36$. The magnitude of the wiggler field is chosen so that the orbit radius of electrons in perfect, $\beta_{||} = \text{const.}$ trajectories is always smaller than the drift tube radius, and thus no decrease in current would have been seen if the electrons had remained in perfect orbits. Consequently the observed decrease in the transmitted current is due to the oscillations around the constant $\beta_{||}$ orbits. Note the general similarity between the behavior of the current and the mismatch velocity, $\Delta\beta_{||\text{I-II}}$, in the region $\Delta\beta_{||\text{I-II}} > 0$ (Fig. 16).

Determination of the transition point between group I and group II orbits provides an interesting test of the three dimensional wiggler theory (Eqs. (8) and (9)) versus one dimensional theory (Eqs. (5) and (7)). For fixed magnetic fields, the electrons will be forced to go from group I to group II orbits as the beam energy γ is lowered (see Figure 5). In general the perpendicular velocity of electrons in group II orbits is much higher than the perpendicular velocity of electrons in group I orbits. As is shown in Fig. 16, there is a sharp drop in the current transmitted through the wiggler at the transition point because the wiggler can be sufficiently strong that electrons in group II orbits are sent into the waveguide wall, and because the mismatch velocity $\Delta\beta_{||\text{I-II}}$ causes the electron orbits to be

very poor.

Experimentally, the transition energy is found (Fig. 17) by firing the Marx bank at a voltage sufficient to ensure that the electrons are initially in group I orbits, and then determing the value of the RC decaying voltage V at which the transmitted current falls to essentially zero. The axial field is held constant at $B_{\|} = 1420\text{G}$ and the wiggler field is varied between 70 and 360G. For the stronger values of wiggler field the insertion conditions are more stringent, and the current begins falling before the transition point is reached. At low wiggler fields the resonance is not strong enough to reduce the current to zero, and the transition point is marked at an energy at which the current drops sharply.

The measured data in Fig. 17 are compared to the transition points predicted by the three dimensional and one dimensional theories. The data agrees well with the three dimensional theory except at very high wiggler fields, where the resonance seems to occur at higher than expected values of energy. The good agreement with three dimensional theory[30] is at first somewhat surprising since the theory assumes that all electrons are in axis encircling electron orbits whose guiding centers are located at $r = 0$. In practice, we have a fairly thick beam ($r_b = 0.254\text{cm}$), and there are many guiding centers well removed from $r = 0$.

At $B_w = 260\text{G}$ the predicted orbit radius $r_\perp = 0.26\text{cm}$ is almost exactly equal to the radius of the beam, and at lower wiggler fields the orbit radius is much smaller than the beam radius. Thus the assumption of axis-encircling orbits is

clearly violated. However numerical simulations show[41] that the three dimensional theory predictions are not only reasonably precise, but are substantially more accurate than the predictions of the one dimensional theory. Indeed, off-axis electrons in realistic wigglers are, in general, found to travel slightly *slower* than predicted by the three dimensional, axis-encircling theory.

The FEL frequency characteristics are studied near resonance by determing the beam energy necessary to amplify a $\omega/2\pi = 12.33\text{GHz}$ signal, as a function of $B_{\|}$, with the wiggler field held constant at $B_w = 190\text{G}$ (Figure 18). Far from resonance the data is obtained by operating the FEL as an amplifier, as described previously. Slightly above resonance spontaneous oscillations preclude amplifier operation and the FEL is run as an oscillator. A 12.33GHz bandpass filter ($\Delta\omega/\omega \approx 0.03$) is used to select the proper frequency.

Well below resonance the required energy is approximately constant, but it increases sharply above $B_{\|} = 2000\text{G}$. At $B_{\|} = 2400\text{G}$ the group I orbit type disappears abruptly and no further increase in the beam energy will result in amplification of the desired frequency. The abrupt termination in the orbit type is reflected in the sudden cessation of the data points.

Well above resonance, the required beam energy is virtually constant until the axial magnetic field is lowered into the resonant region. The vertical lines in Fig. 18 indicate that in this region of $B_{\|}$ and γ, in which $\Phi < 0$, the frequency $\omega/2\pi = 12.33\text{GHz}$ is emitted over a broad range of electron energies. This implies

that for a given fixed beam energy, radiation would be emitted over a wide frequency band, in accordance with theoretical predictions.[5,36] Occasionally in the region 3000G $< B_{||} <$ 3400G, we observe radiation which we attribute to the cyclotron maser instability, whose presence is always a worrisome possibility.[40]

V—Discussion

Experiments using tenuous, highly relativistic electron beams[42–45] have clearly demonstrated the concept of the single particle, Compton free electron laser. The high current collective Raman free electron laser, however has not been so readily demonstrated. Early experiments have suggested that the Raman free electron laser configuration can generate tunable,[8,46] high frequency,[13] intense[31] radiation, but work on Raman FELs has been impeded by problems associated with the generation, transmission, and diagnosis of high quality electron beams, technical difficulties with the measurements of very short radiation pulses, and competition from other instabilities. Much of this has now changed, and recent experiments[9,32,33,47,48] use good quality electron beams in carefully controlled experimental setups.

In our experimental study presented here we investigate the basic properties of the free electron laser instability and compare our results to various theoretical models. Our FEL operates in the mildly relativistic (Ubitron) regime of electron energies ($V \sim$ 160kV) with beam currents normally ranging from 1—8A, but occasionally as large as 48A. The thermionic cathode immersed in the field

of several carefully designed beam focusing coils produces a low ($\Delta\gamma_{\|}/\gamma \simeq 3\times10^{-3}$) temperature beam. This, together with a sufficiently high current density ($> 20\text{A cm}^{-2}$) ensures operation in the collective Raman regime.[1,2] Furthermore, the thermionic cathode permits one to operate the FEL as a long pulse device ($0.2-2\mu\text{s}$). This is in contrast to most,[12–14] but not all,[46,47] Raman FEL experiments in which diode closure of the field emission diode limits the pulse length to $\sim 100\mu\text{s}$ or less.

We use our FEL both as an oscillator and as an amplifier. With the above quoted beam temperature, we observe in the oscillator mode 100kW of RF power at a current of $\sim$ 5A. This corresponds to an electronic efficiency of 12% of converting beam energy to radiation. When the current is increased to 50A, with relaxed beam quality, as much as $\sim$ 1MW of RF power is observed, albeit at a reduced efficiency of $\sim$ 8%. This illustrates the importance of beam quality,[38] a fact that was not realized in the very early experiments.[8,13] The measured bandwidth $\Delta\omega/\omega$ equals approximately 0.02, except just above resonance, $\Omega_{\|}/\gamma > k_w\beta_{\|}c$, where broad band emission occurs, in agreement with predictions.[5,36] The observed radiation is excited in a single TE_{11} waveguide mode of the cylindrical drift tube which also acts as the waveguide.

When our FEL is used as an amplifier, single pass gain of 20dB is achieved. The system is voltage tunable over a continuous frequency range from 7 to 21GHz, and confirms the promise[16] of wide tunability by changing the accelerator

voltage alone. This differs from frequency tuning obtained by variation of the wiggler field amplitude[31,33] which must be adopted when voltage tuning is not feasible. Tuning by variation of B_w is less desirable since changing B_w also varies the FEL gain.

Our studies are conducted over a variety of axial magnetic fields, well below, well above, and close to resonance $\Omega_{\|}/\gamma \simeq k_w\beta_{\|}c$. Good performance at guide magnetic fields just large enough to keep the beam focused ($\sim$ 1600G) is a particularly satisfactory result, since low guide fields, or, for that matter, no guide magnetic fields, are mandatory for purposes of scaling the FEL to submillimeter wavelengths. As an example, an FEL designed to operate at a wavelength of 100μm with a 3MV electron beam would, if operated above resonance, require a guide field exceeding $\sim$ 100kG. For that reason a number of studies[14,31,32] conducted at high guide fields $\Omega_{\|}/\gamma > k_w\beta_{\|}c$ are not scalable to submillimeter wavelengths.

The presence of a strong guide magnetic field has an additional disadvantage in that it allows for the possible excitation of other instabilities, particularly the cyclotron maser instability.[40] This is always a troublesome possibility, especially near resonance[14,31] where the radiation frequencies of the FEL and cyclotron masers begin to approach one another closely. For this reason, many of the recent FEL experiments avoid the presence of guide magnetic fields in the wiggler region.[33,47] Our studies have shown that complete elimination of $B_{\|}$ in the wiggler

is unnecessary.

Finally we note the excellent agreement found between measurements and theory, both far and near to resonance. Whenever there is a clear difference between one and three dimensional FEL theory, our measurements indicate better agreement with the latter, in disagreement with earlier assertions.[31] We believe that ours is the first study that has undertaken a detailed comparison between observations and the latest theoretical developments.[10,11]

Acknowledgments

We thank Achintya Ganguly and Henry Freund for use of their computer code, and for their helpful explanations. This work was supported in part by the National Science Foundation, in part by the Hertz Foundation, in part by the Air Force Office of Scientific Research, and in part by the Air Force Aeronautical Systems Division (AFSC).

References

[1] P. Sprangle, R. A. Smith, and V. L. Granatstein, *Infrared and Millimeter Waves,* K. J. Button, ed. Vol. 1, Academic Press, N.Y., 279 (1979), and references therein.

[2] N. M. Kroll, and W. A. McMullin, W. A., *Phys. Rev. A.* **17**, 300 (1978).

[3] J. A. Davies, R. C. Davidson, and G. L. Johnston, *M. I. T. Plasma Fusion Center Report,* PFC/JA-84-11, (May, 1984).

[4] L. Friedland, *Phys. Fluids.* **23**, 2376 (1980).

[5] L. Friedland and A. Fruchtman, *Phys. Rev. A.* **25**, 2693 (1982).

[6] H. P. Freund and P. Sprangle, *Phys. Rev. A.* **28**, 1835 (1983).

[7] W. McMullin, and R. C. Davidson, *Phys. Rev A.* **25**, 3130 (1982).

[8] M. Phillips, *IRE Trans. Elect. Dev.* **ED-7**, 231 (1960), also C. E. Enderby and R. M. Phillips, *Proc. of the IEEE* **53, 1648 (1965).**

[9] J. Fajans, G. Bekefi, Y. Z. Yin, and B. Lax, *Phys. Rev. Lett..* **53**, 246 (1984).

[10] H. P. Freund and A. K. Ganguly, *Phys. Rev. A.* **28**, 3438 (1983).

[11] H. S. Uhm and R. C. Davidson, *Phys. Fluids.* **24**, 2348 (1981).

[12] R. H. Jackson, S. H. Gold, R. K. Parker, H. P. Freund, P. C. Efthimion, V. L. Granatstein, M. Herndon, A. K. Kinkead J. E. Kosakowski, and T. J. Kwan, *IEEE J. Quant. Elect.* **QE-19**, 346 (1983).

[13] T. C. Marshall, S. P. Schlesinger, and D. B. McDermott, *Adv. Elect. Physics.* **53**, 47 (1980), and references therein.

[14] K. L. Felch, L. Vallier, J. M. Buzzi, P. Drossart, H. Boehmer, H. J. Doucet, B. Etlicher, H. Lamain, C. Rouille, *IEEE J. Quant. Elect.* **QE-17**, 1354 (1981).

[15] J. R. M. Vaughan, *IEEE Trans. Elect. Devices.* **ED-21**, 310 (1974).

[16] P. Diament, *Physical Review A.* **23**, 2537 (1981).

[17] W. B. Herrmannsfeldt, *Stanford Linear Accelerator Center,* SLAC-226, (November, 1979).

[18] R. E. Shefer, Y. Z. Yin, and G. Bekefi, *J. Appl. Phys.* **54**, 6154 (1983).

[19] R. C. Davidson, *Theory of Nonneutral Plasmas,* W. A. Benjamin, Reading, (1974).

[20] V. K. Neil, *Jason Technical Report,* JSR-79-10, (December 1979).

[21] J. Fajans, G. Bekefi, B. Lax, *Proc. IEEE Conference on Plasma Science, Ottawa.* 18 (1982).

[22] J. R. Thompson and M. L. Sloan, *Phys. Fluids.* **21**, 2032 (1978).

[23] H. Poritsky, *J. Appl. Phys..* **30**, 1828 (1959).

[24] B. Kincaid, *J. Appl. Phys..* **48**, 2684 (1977).

[25] J. R. Blewett, R. Chasman, *J. Appl. Phys..* **48**, 2692 (1977).

[26] J. Fajans, *J. Appl. Phys.* **55**, 43 (1984).

[27] G. M. Branch, and T. G. Mihran, *IRE Trans. Elect. Dev.* **ED-2**, 3 (1955), the formulas given here must be corrected for relativistic effects.

[28] R. E. Trotman, *Longitudinal Space Charge Waves,* Chapman and Hall, London, (1966).

[29] A. Gover, and P. Sprangle, *IEEE J. Quant. Elect..* **QE-17**, 1196 (1981).

[30] H. P. Freund, S. Johnston, P. Sprangle, *IEEE J. Quant. Elect.*. **QE-19**, 322 (1983).

[31] S. H. Gold, W. M. Black, H. P. Freund, V. L. Granatstein, R. H. Jackson, P. C. Efthimion, and A. K. Kinkead, *Phys. Fluids.* **26**, 2683 (1983).

[32] S. H. Gold, D L. Hardesty, A. K. Kinkead, L. R. Barnett, and V. L. Granatstein, *Phys. Rev. Lett.*. **52**, 1218 (1984).

[33] T. J. Orzechowski, B. Anderson, W. M. Fawley, D. Prosnitz, E. T. Scharlemann, S. Yarema, D. Hopkins, A. C. Paul, A. M. Sessler and J. Wurtele, *Lawrence Livermore National Laboratory,* Report No. UCRL-91559, (1984).

[34] H. P. Freund, Private communication.

[35] A. Hasegawa, *Bell Syst. Tech. J.* **57**, 3069 (1978).

[36] H. P. Freund, P. Sprangle, D. Dillenburg, E. H. da Jornada, R. S. Schneider, and B. Liberman, *Phys. Rev. A.* **26**, 2004 (1982).

[37] W. McMullin, , Ph.D thesis, Dept. of Physics, University of California, San Diego, (1980).

[38] T. J. T. Kwan and C. M. Snell, *Phys. Fluids.* **26**, 835 (1983).

[39] T. J. Orzechowski, and G. Bekefi, *Phys. Fluids.* **22**, 978 (1979).

[40] R. E. Shefer and G. Bekefi, *Int. J. Electronics.* **51**, 569 (1981).

[41] D. A. Kirkpatrick, Private communication.

[42] J. A. Edighoffer, G. R. Neil, C. E. Hess, T. I. Smith, S. W. Fornaca, and H. A. Schwettman, *Phys. Rev. Lett.* **52**, 344 (1984), and references therein.

[43] M. Billardon, P. Elleaume, J. M. Ortega, C. Bazin, M. Bergher, M. Velghe, Y. Petroff, D. A. G. Deacon, K. E. Robinson, and J. M. J. Madey, *Phys. Rev. Lett.* **51**, 1652 (1983).

[44] R. W. Warren, B. E. Newnam, J. G. Winston, W. E. Stein, L. M. Young, C. A. Brau, *IEEE J. Quant. Elect.* **QE-19**, 391 (1983).

[45] *Phys. Today.* **37**, American Institute of Physics, 21 (1984).

[46] H. Boehmer, M. Z. Caponi, J. Munch, *IEEE Trans. Nucl. Sci.* **NS-26**, 3830 (1979), also Proceedings Sicily Workshop-Erice, August 1980.

[47] J. A. Pasour, R. F. Lucey, and C. A. Kapetanakos, *Phys. Rev. Lett.* **53**, 1728 (1984).

[48] J. Masud, T. C. Marshall, and S. P. Schlesinger, *Bull. Am. Phys. Soc.* **29**, 1341 (1984).

Figures

Figure. 1 Schematic of the free electron laser.

Figure. 2 Simulation of the electron gun for $V = 250\text{kV}(\gamma = 1.49)$, and $B_{\|} = 1500\text{G}$. Only one fifth of the electron trajectories are shown. The dashed rectangle indicates the dimension of the beam aperture placed further down the drift tube. Note the gentle scalloping of the beam radius.

Figure. 3 Fractional transverse energy spread as a function of the normalized axial magnetic field. Experimental data are for $\gamma = 1.42$ and the simulations are for $\gamma = 1.50$. Transverse and axial energy spreads are related through $\Delta E_{\perp}/E = \Delta\gamma_{\|}/\gamma$.

Figure. 4 Measured profile of the wiggler field strength as a function of axial position at the upstream end of the wiggler. Both wiggler polarizations were measured and used to determine the wiggler magnitude; for clarity only one polarization is shown.

Figure. 5 Variation of the axial velocity $\beta_{||}$ with energy γ for fixed axial and wiggler magnetic fields calculated from Eqs. (6) and (7); I and II indicate the Group I and Group II orbits. The dashed lines are inaccessible for constant $\beta_{||}$ orbits.

Figure. 6 Typical oscilloscope traces showing the beam voltage and current, and the microwave power, in the oscillator mode.

Figure. 7 (a) Microwave power as a function of wiggler amplitude B_w in the oscillator mode. (b) The triangles give the beam energy at which maximum power is observed for each of the points in (a). The line is the theoretically predicted energy at the point of maximum growth (grazing intersection of the upshifted plasma wave and the TE_{11} waveguide mode.)

Figure. 8 (a) Dispersive line data in the oscillator mode showing the undispersed signal (R) and the high frequency dispersed mode (I); (b) shot for the case where both the high (I) and the low frequency modes (II) are present simultaneously.

Figure. 9 Radiation frequency measured with the dispersive line, as a function of beam voltage V in the oscillator mode. The horizontal arrow denotes the cutoff frequency of the TE_{11} mode. Experimental error in the measured quantities is less than two percent. Tuning is also achieved by variation of B_w at constant V.

Figure. 10 Measurements in the amplifier mode. (a) Time history of the beam voltage V; (b) 1 marks is the amplitude of a 8.2GHz injected signal; 2 marks the amplified FEL signal; 3 marks the damped fast space charge mode (see text)

Figure. 11 Power out vs. power in for a fixed set of FEL parameters as measured in the amplifier mode. The system gain is approximately 9dB. Statistical error bars are shown for a typical point.

Figure. 12 Amplifier system response to a train of microwave pulses. The length of each pulse is less than the system bounce time, so that the observed gain is due to single pass amplification.

Figure. 13 Gain as a function of wiggler strength. The solid line is from the three dimensional theory.[10]

Figure. 14 Radiation frequency as a function of beam voltage V with the FEL in the amplifier configuration. (a) Below resonance ($\Omega_{\|}/\gamma < k_w\beta_{\|}c$); (b) above resonance ($\Omega_{\|}/\gamma > k_w\beta_{\|}c$). The horizontal arrows denotes the cutoff frequency of the TE_{11} mode.

Figure. 15 Beam energy γ required to amplify radiation at $f = 12.02\text{GHz}$ as a function of beam plasma frequency. Data shown by dots in (a) are below resonance, and in (b) above resonance. In both cases $B_w = 166\text{G}$. The solid line is from theory. The squares represent the damped, fast space charge wave interaction; and the dashed line is from theory.

Figure. 16 (a) Total normalized velocity β_{tot}, perpendicular velocity $\beta_{\perp}$ and mismatch velocity $\Delta\beta_{\|}$ I-II versus energy γ for fixed magnetic fields. (b) Measurement of current I transmitted through the wiggler as a function of energy γ for fixed magnetic fields.

Figure. 17 Measured beam energy at the group I–II transition (see Fig. 16a), as a function of wiggler strength compared to the predictions of the one dimensional and three dimensional theories.

Figure. 18 Beam energy γ required for radiation at $f = 12.33\text{GHz}$ as a function of axial magnetic field $B_{\|}$, both far from and near to resonance ($\Omega_{\|}/\gamma = k_w \beta_{\|} c$). The solid lines are from theory. The long vertical lines signify broadband operation (see text).

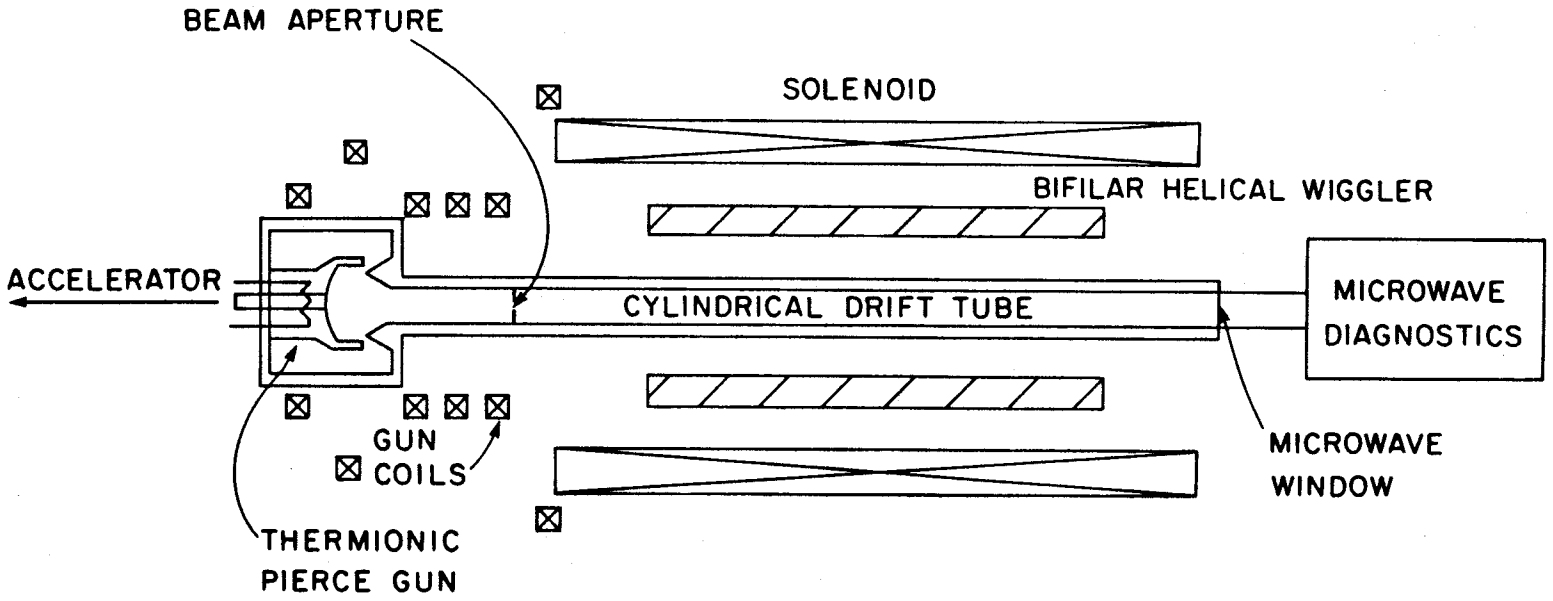

Fig. 1
Fajans, Bekefi, Yin, Lax

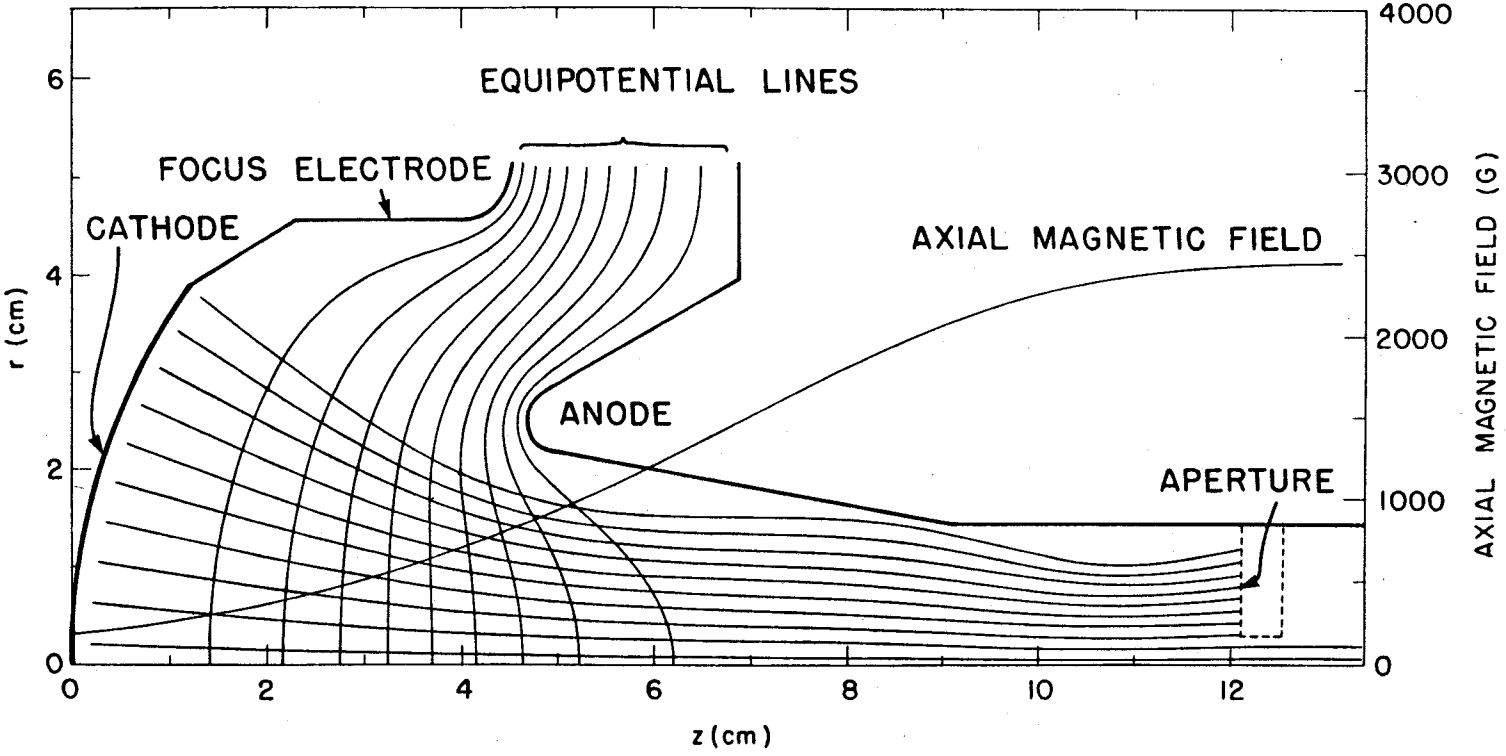

Fig. 2
Fajans, Bekefi, Yin, Lax

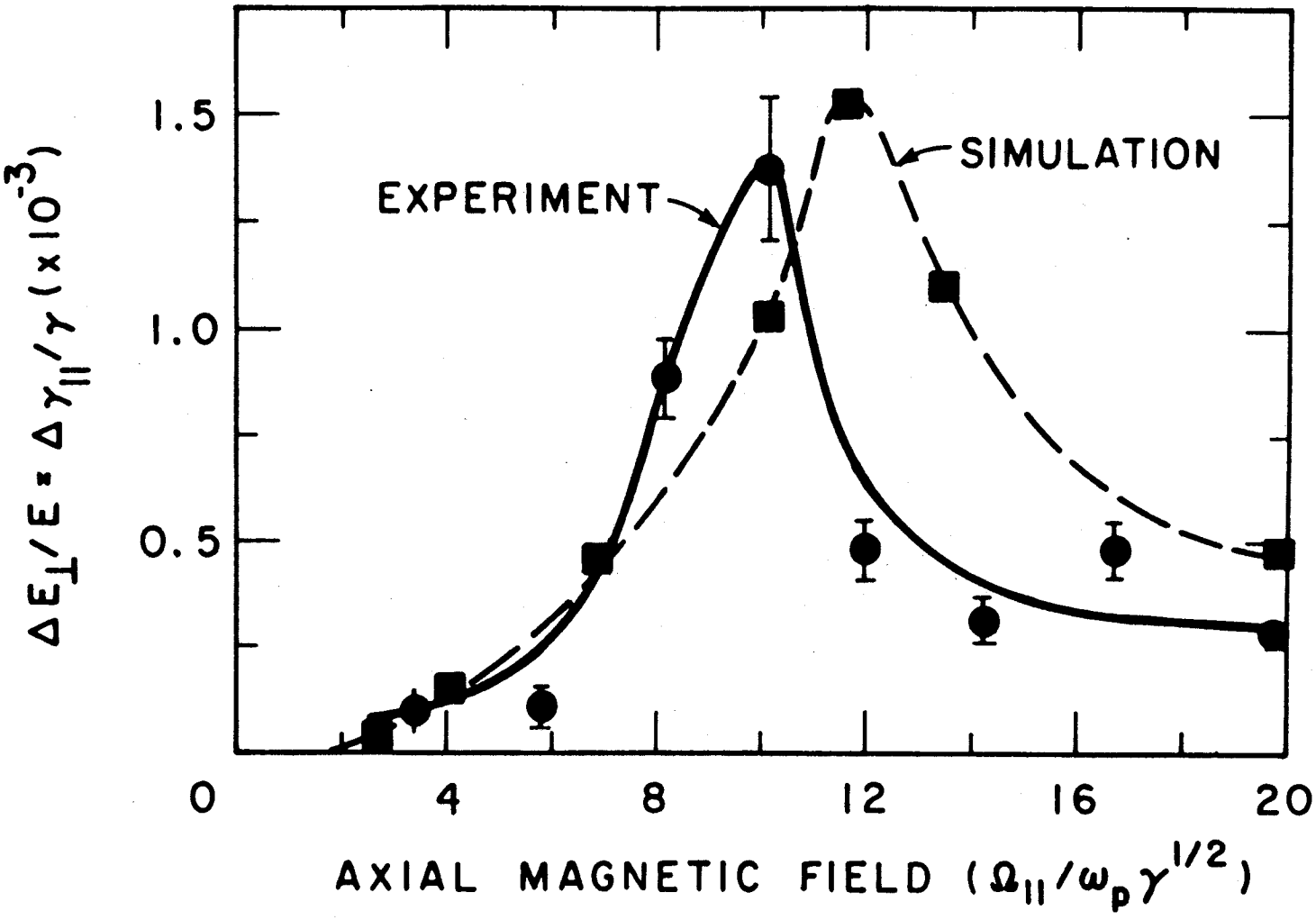

Fig. 3
Fajans, Bekefi, Yin, Lax

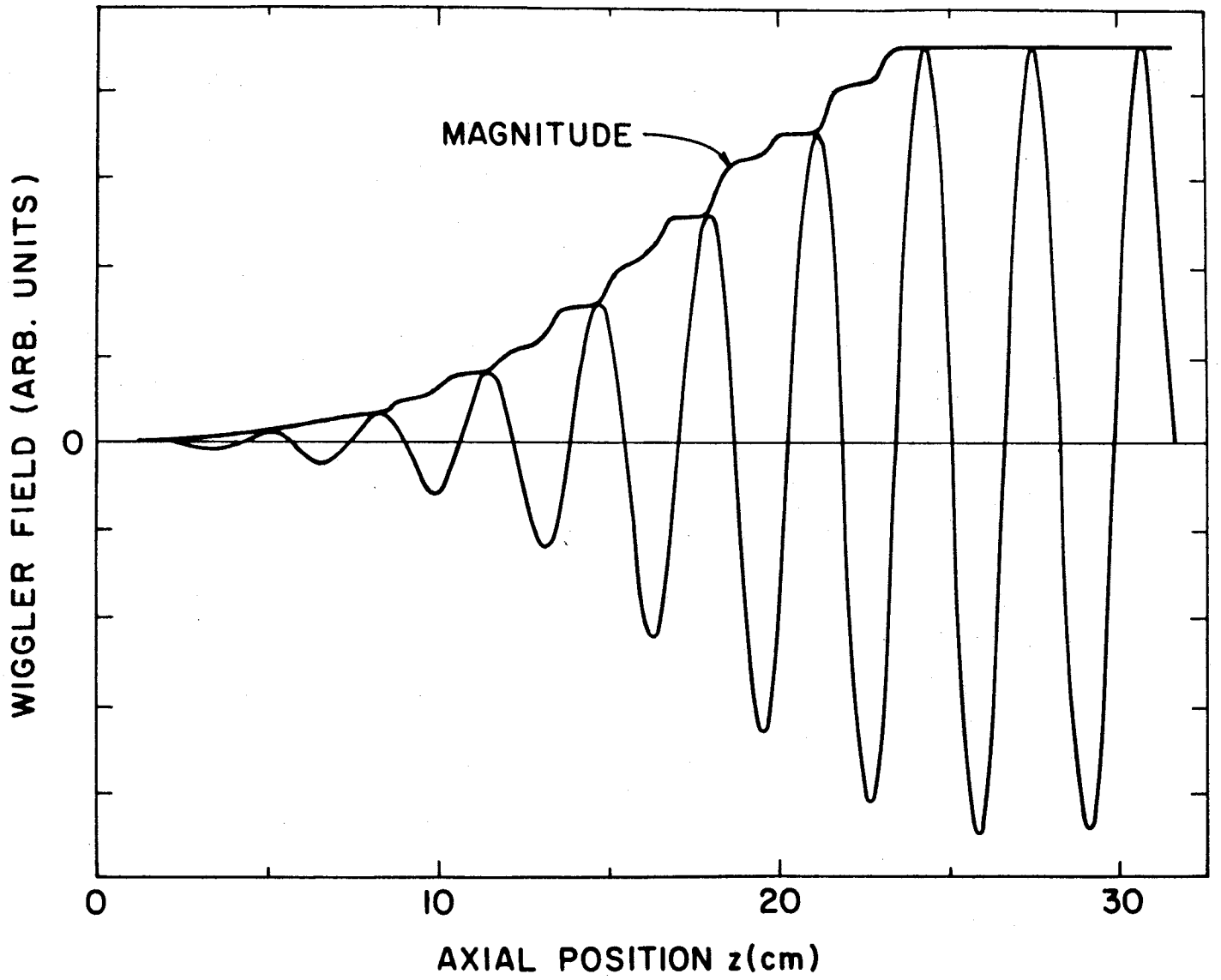

Fig. 4
Fajans, Bekefi, Yin, Lax

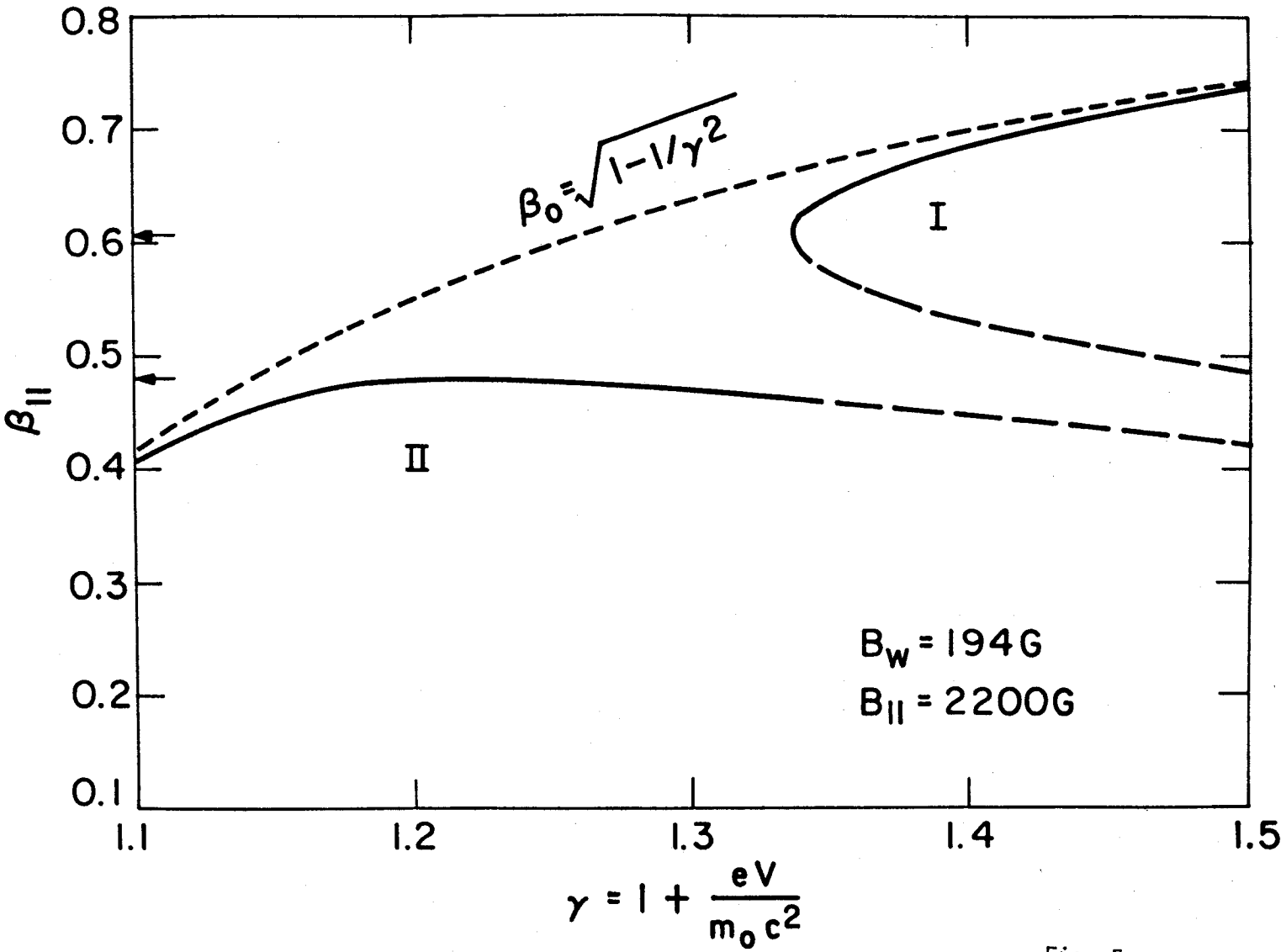

Fig. 5
Fajans, Bekefi, Yin, Lax

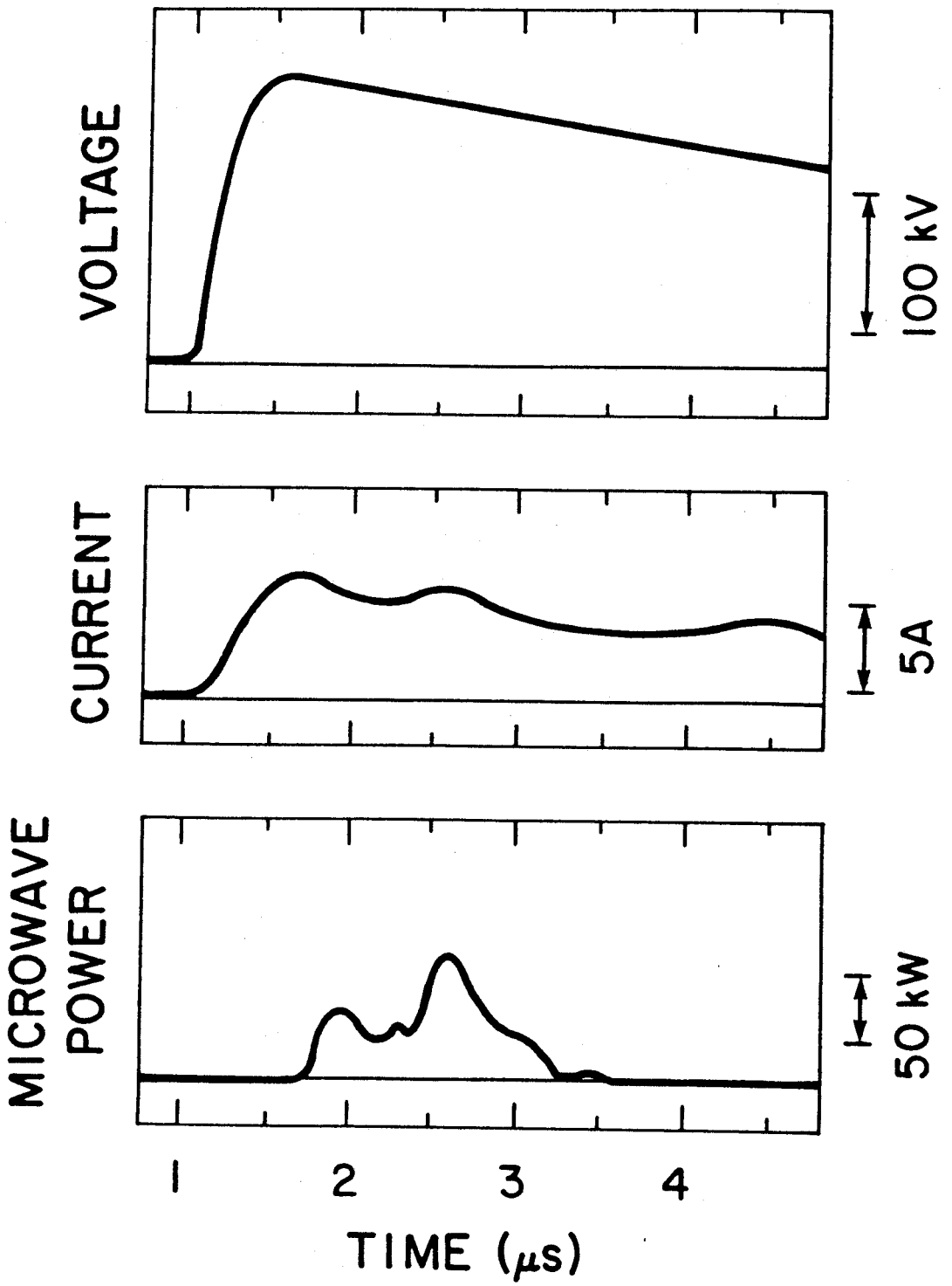

Fig. 6
Fajans, Bekefi, Yin, Lax

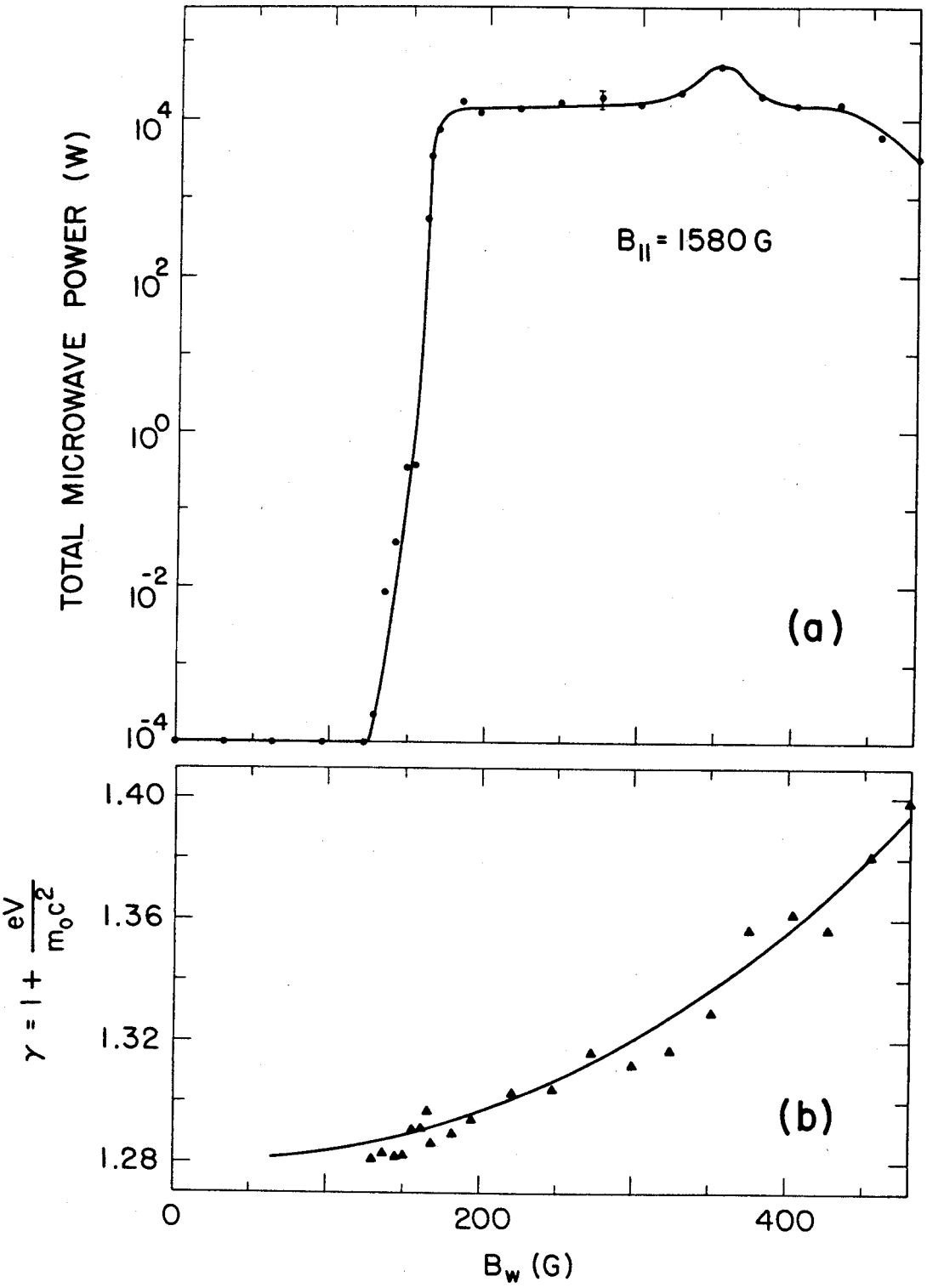

Fig. 7
Fajans, Bekefi, Yin, Lax

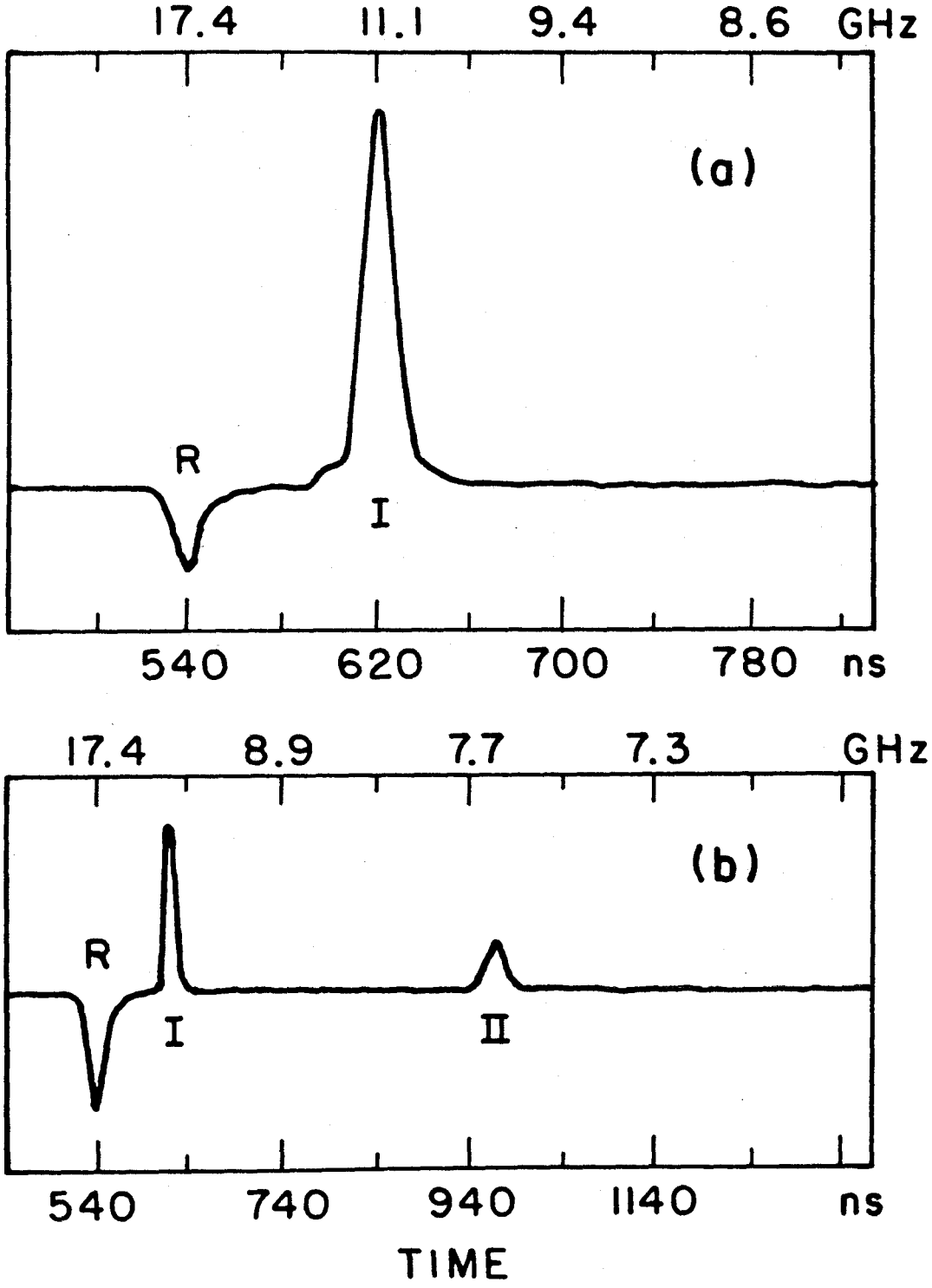

Fig. 8
Fajans, Bekefi, Yin, Lax

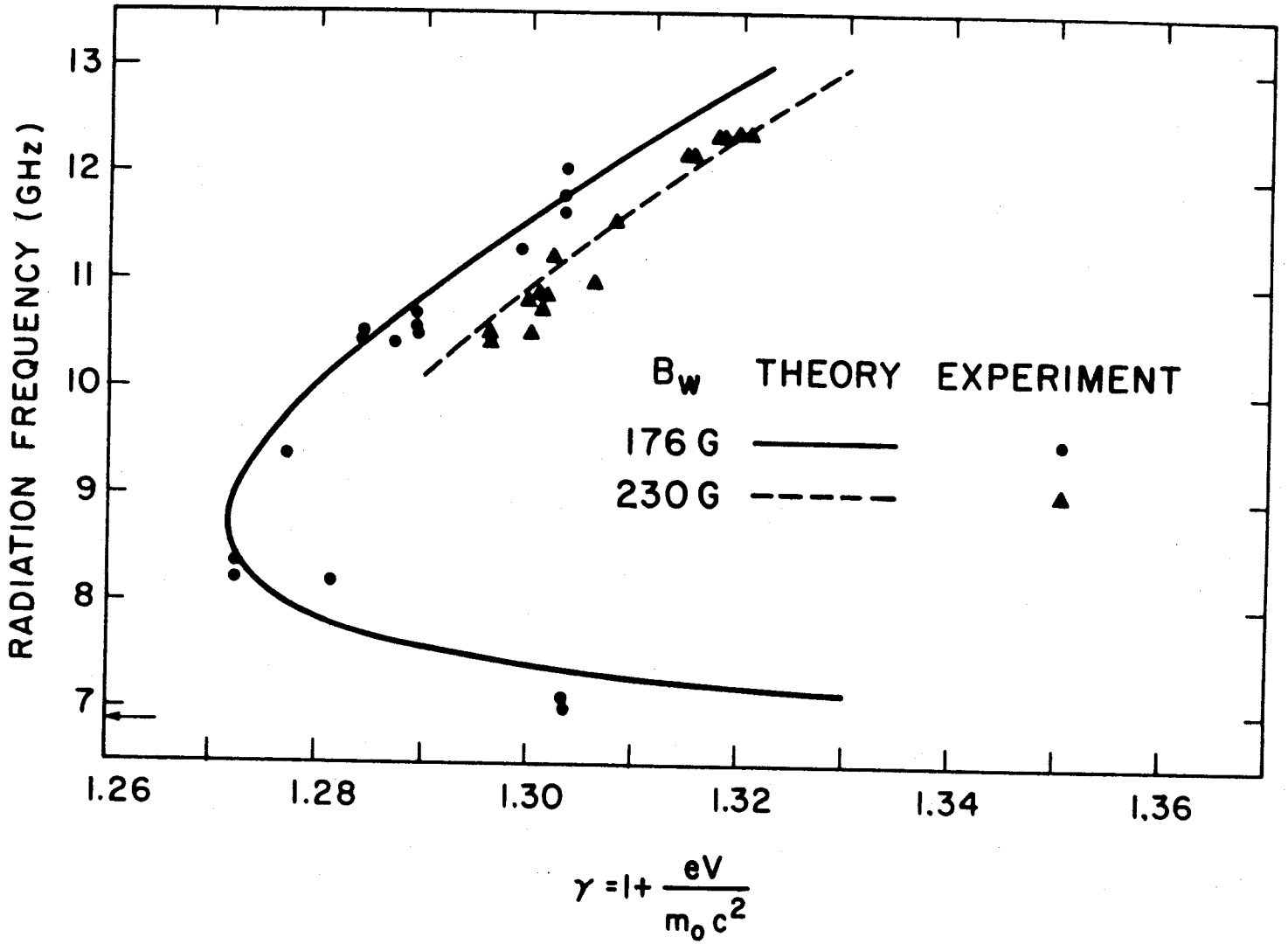

Fig. 9
Fajans, Bekefi, Yin, Lax

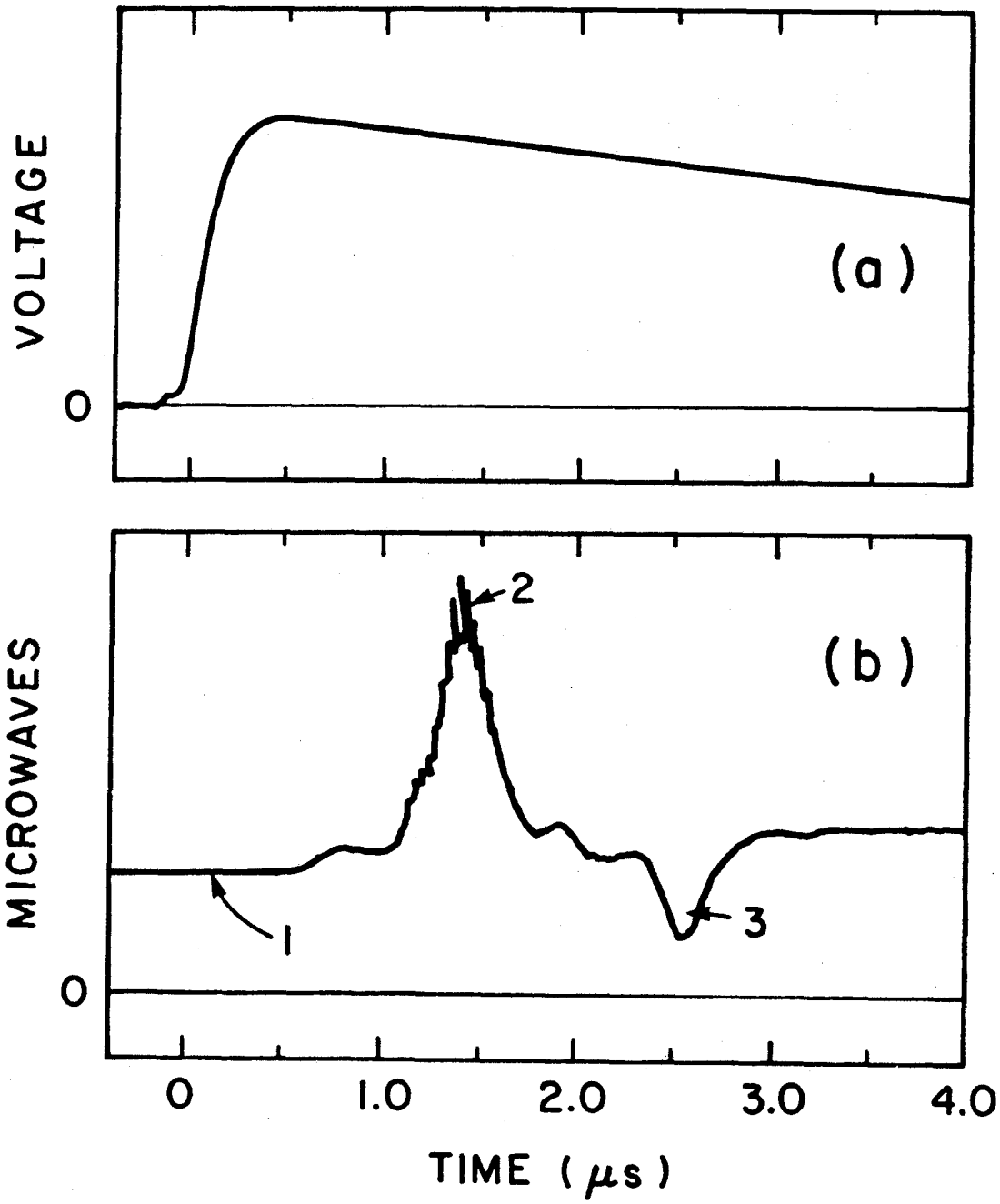

Fig. 10
Fajans, Bekefi, Yin, Lax

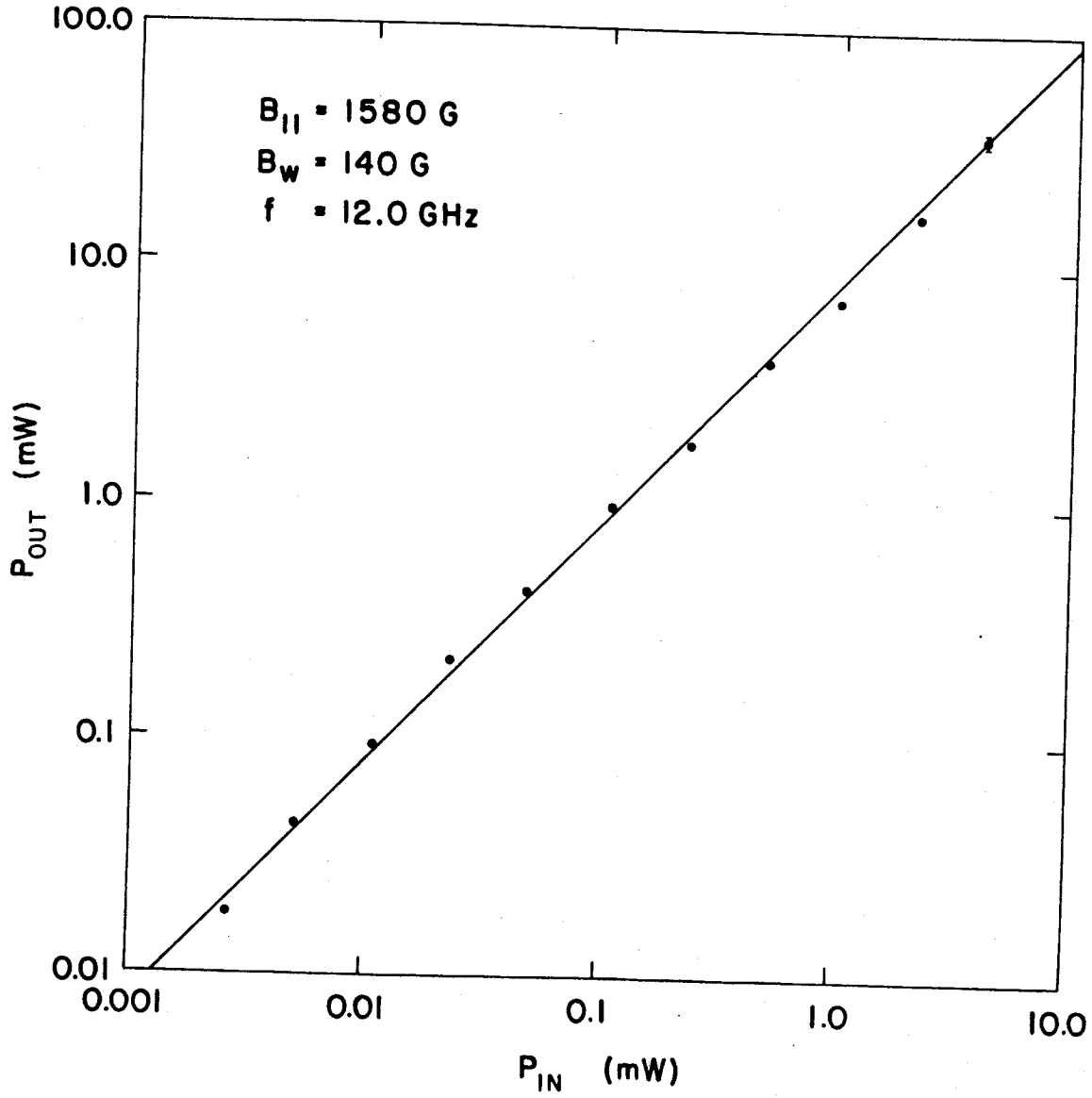

Fig. 11
Fajans, Bekefi, Yin, Lax

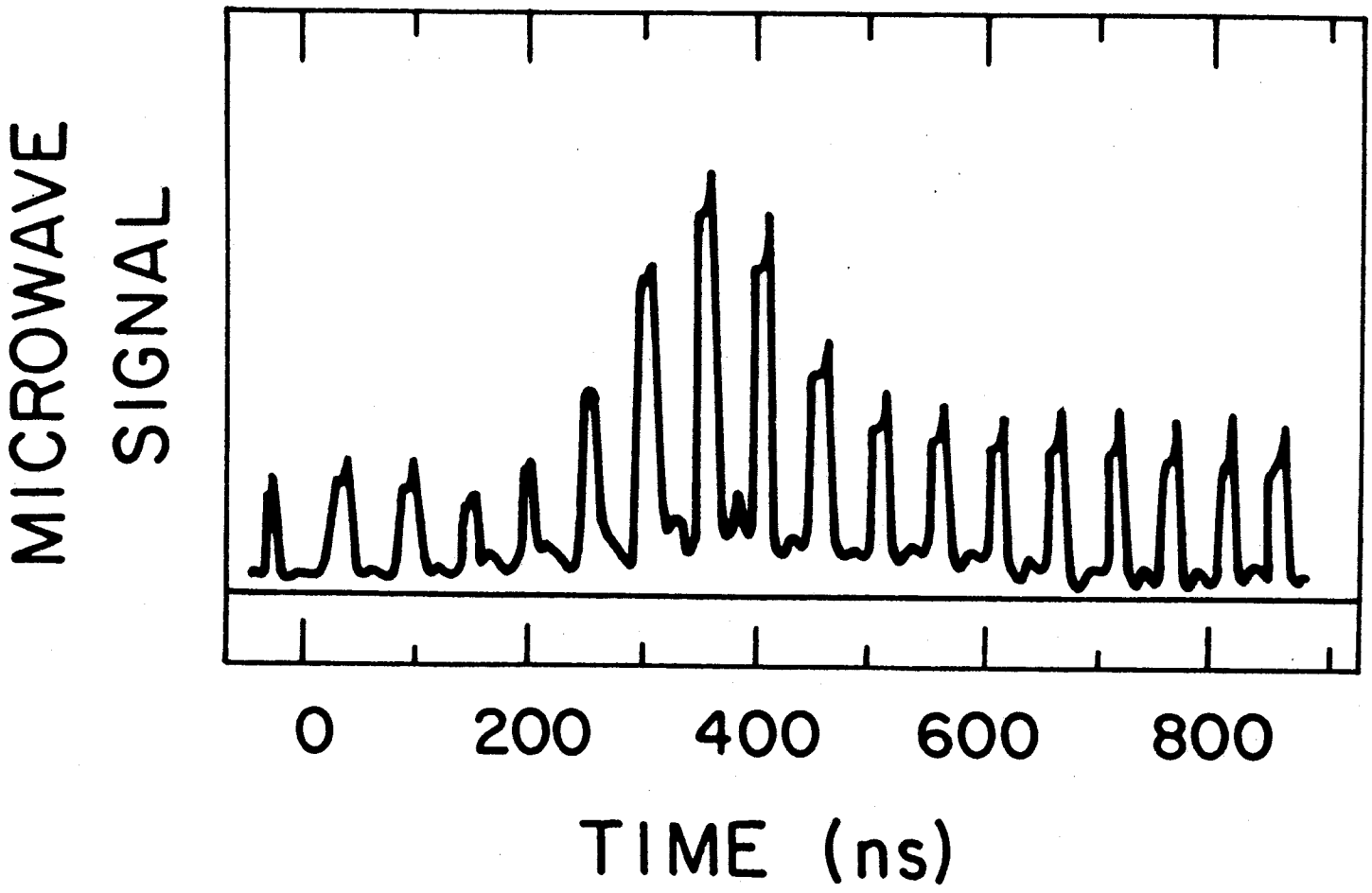

Fig. 12
Fajans, Bekefi, Yin, Lax

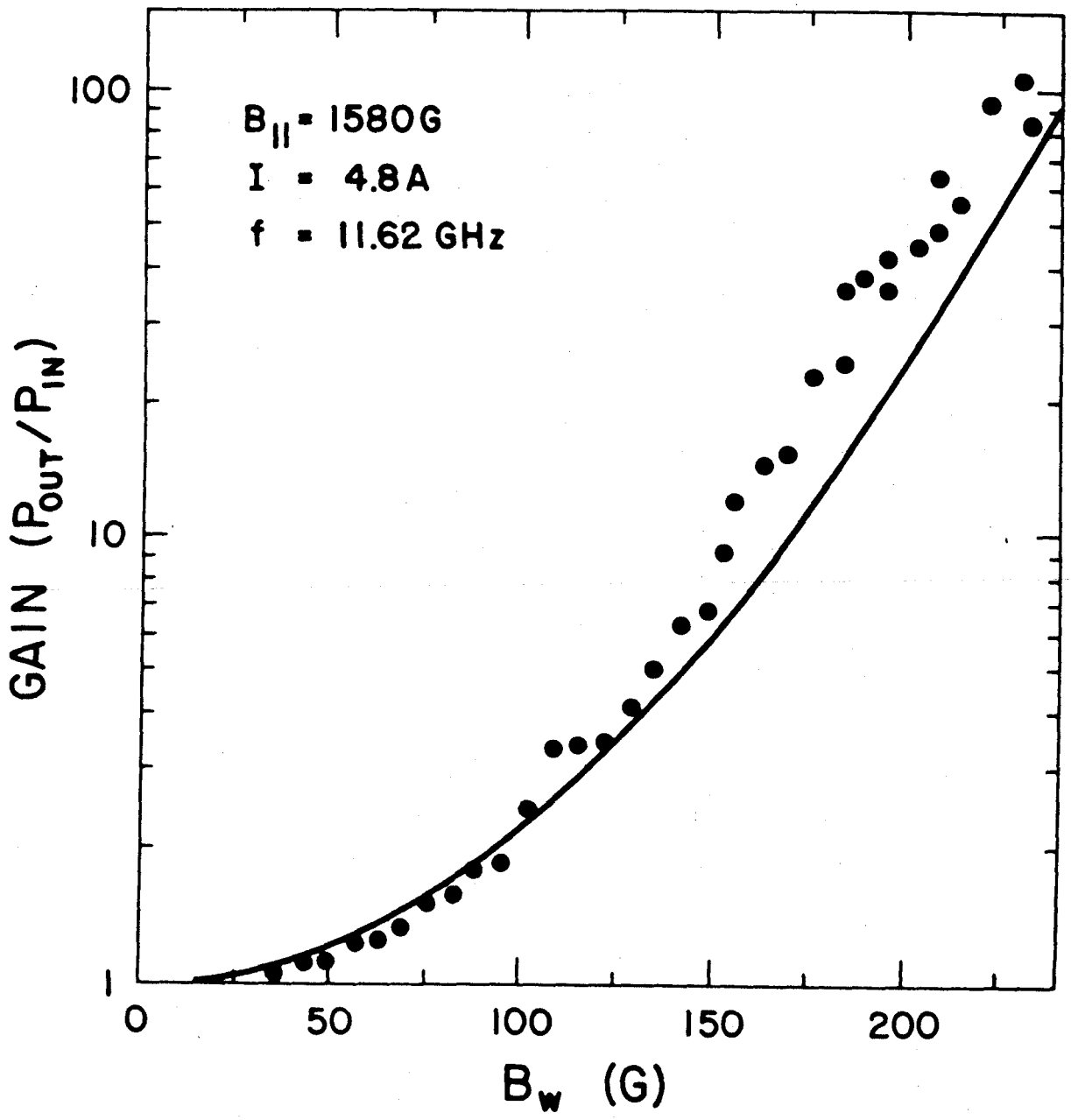

Fig. 13
Fajans, Bekefi, Yin, Lax

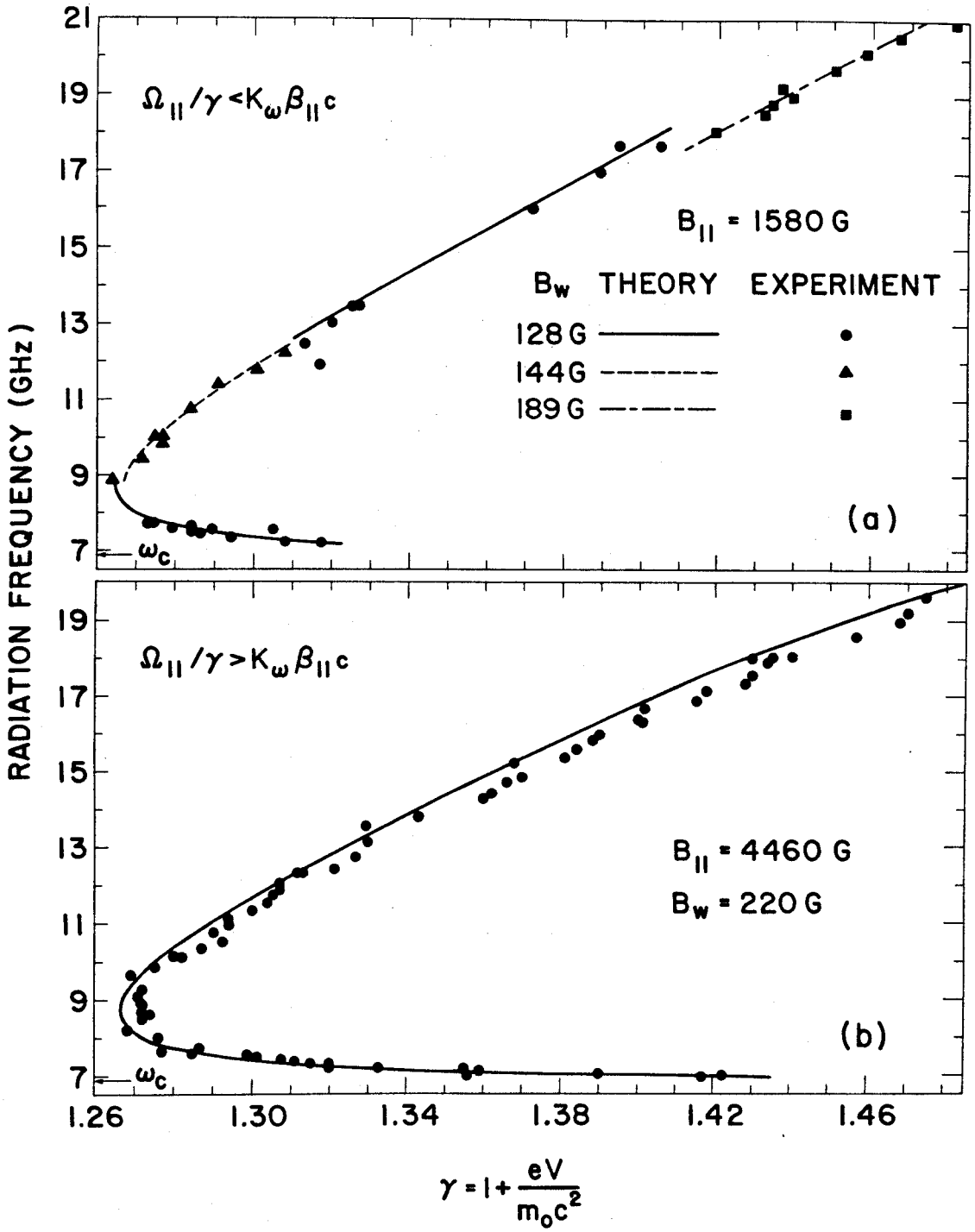

Fig. 14
Fajans, Bekefi, Yin, Lax

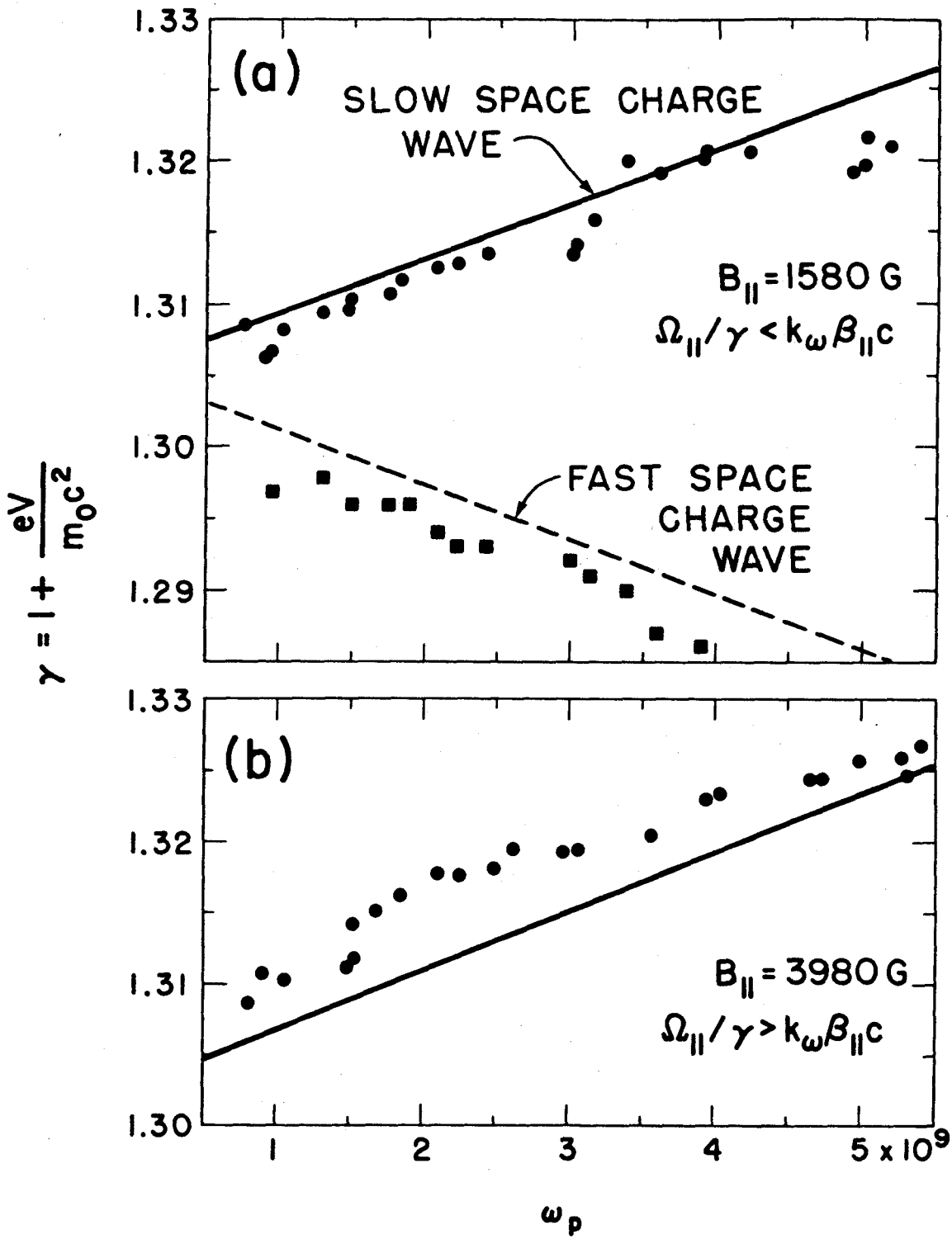

Fig. 15
Fajans, Bekefi, Yin, Las

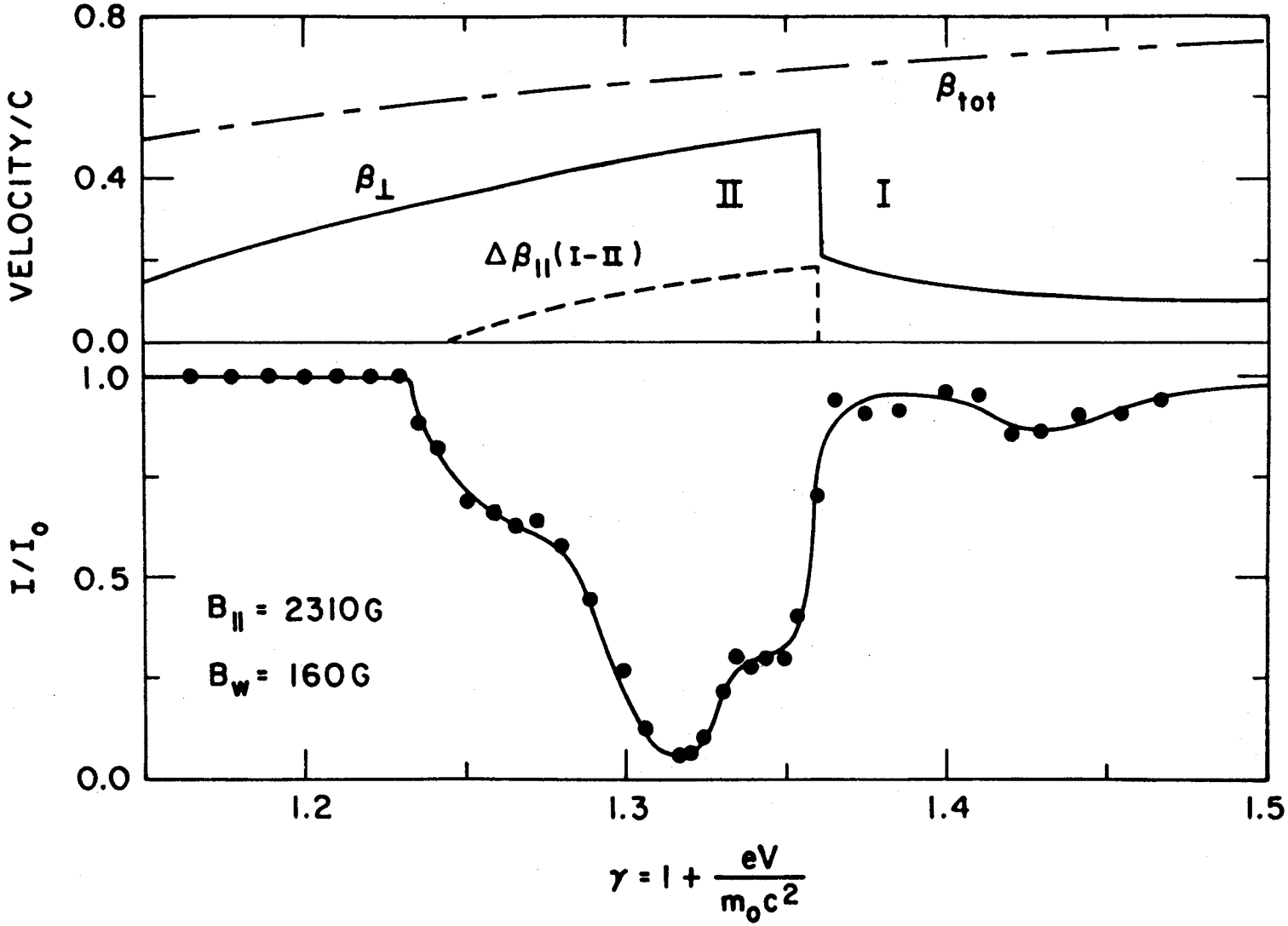

Fig. 16
Fajans, Bekefi, Yin, Lax

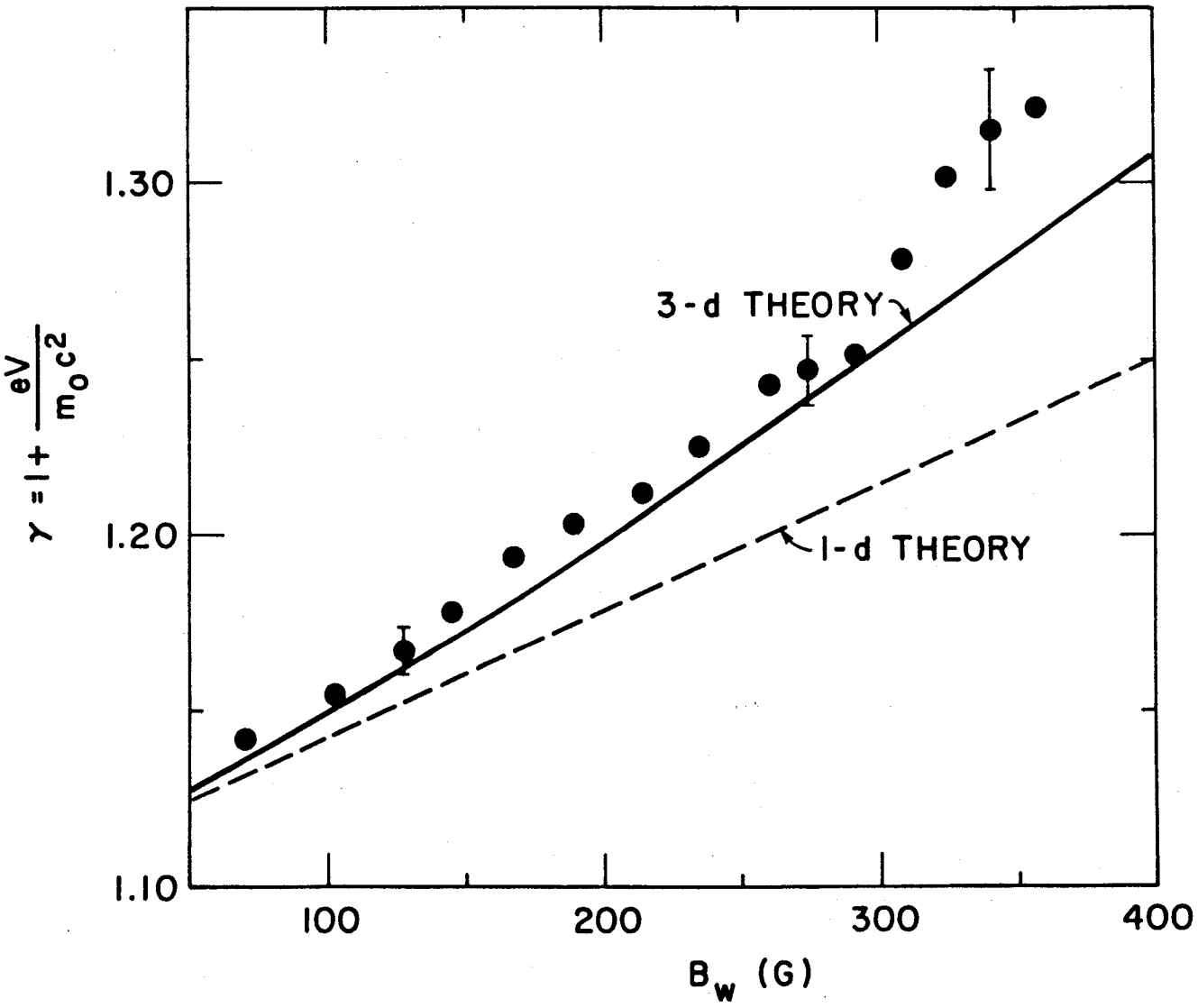

Fig. 17
Fajans, Bekefi, Yin, Lax

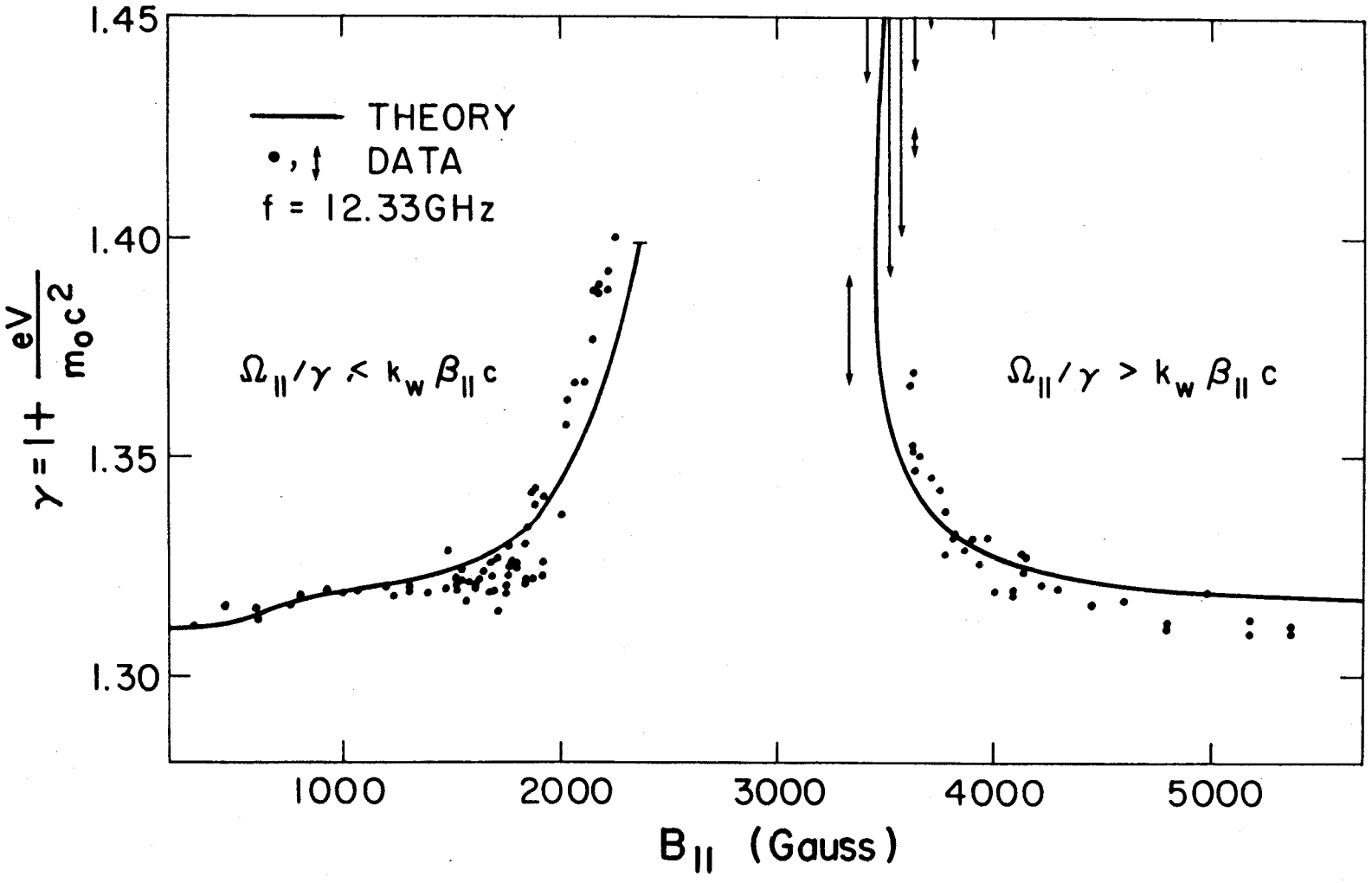

Fig. 18
Fajans, Bekefi, Yin, Lax